Online UHF Measurement of Partial Discharge in Stator Windings Using Microstrip Patch Antennas

by

Michael Denis Joseph Partyka

A thesis submitted to the Faculty of Graduate Studies of
The University of Manitoba
in partial fulfilment of the requirements of the degree of

Master of Science

Department of Electrical and Computer Engineering
University of Manitoba
Winnipeg, Canada

Examining Committee

This thesis was examined and approved by the following examining committee on December 16, 2019:

- **Dr. G. Bridges** (advisor)
  Department of Electrical & Computer Engineering
  University of Manitoba
- **Dr. B. Kordi** (co-advisor)
  Department of Electrical & Computer Engineering
  University of Manitoba
- **Dr. P. Mojabi**
  Department of Electrical & Computer Engineering
  University of Manitoba
- **Dr. N. Fernando**
  Department of Electrical & Computer Engineering
  University of Manitoba

Abstract

Partial Discharge (PD) is the electrical discharge resulting from the partial dielectric breakdown of voids in electrical insulation. PD is a phenomenon that can be measured from conducted currents or radiated emissions and can be used to help evaluate the condition of rotating machine winding insulation. PD occurs in stator winding groundwall insulation due to the voltage stress in voids left by the manufacturing process, but it also occurs when other defects are present in the insulation system. PD from each type of defect in a stator winding produces a unique phase resolved partial discharge (PRPD) pattern which is presented as a plot of PD pulse magnitude against power frequency phase. Using PRPD patterns, different stator winding defects can be characterized by PD pulse polarity, phase location, and cluster shape.

On stator windings, it is typical to perform online PD measurements in the VHF range using high voltage capacitors to couple high frequency currents from the generator's ring bus, terminals, or isolated phase bus. It is also typical to perform online PD measurements in the UHF range with near-field sensors placed underneath stator slot wedges which couple induced PD currents. Existing stator winding PD measurement systems require a machine outage for installation which can be prohibitively expensive. It would be advantageous to use antennas for online PD measurements since no outage would be required and installation

would be simple. Currently, there is not enough existing research to determine whether antenna-based methods are feasible.

This thesis investigates antenna-based UHF techniques for online PD measurements. Rectangular microstrip patch antennas were designed and fabricated with resonant frequencies of 900, 1500, and 2450 MHz. These antennas were used to detect and quantify PD on single Roebel bars in a laboratory setting and on the stator winding of an operating hydrogenerator. This was done by placing each antenna near the specimens, acquiring pulses with a digital oscilloscope, and presenting PRPD patterns from these acquisitions. Based on the agreement between PRPD patterns from these tests and those obtained with a commercial instrument, PD was successfully measured with the antennas on every specimen.

Acknowledgements

My advisors Drs. Greg Bridges and Behzad Kordi have both dedicated a significant amount of time meeting with me, reviewing my work, and leading me in the right direction. I appreciate their patience and understanding as I slowly worked through this degree on a part time basis. They have been great to work with and allotted me quite a bit of freedom in regards to the direction of this thesis.

I would like to thank everyone at the High Voltage Test Facility for supporting me throughout this endeavor. I would especially like to thank Tyler Black and Bill McDermid who taught me much of what I know in regards to high voltage testing. Without being affiliated with me academically in an official sense, they both reviewed my work, provided direction, and inspired me to make a thesis that was practical.

I would like to thank Drs. Puyan Mojabi and Namal Fernando for agreeing to join the examining committee with my advisors. They have already had an impact on this thesis. Dr. Mojabi taught my undergraduate antennas class and Dr. Fernando has been the manager of Manitoba Hydro's High Voltage Test Facility since I started working there in 2016.

I am grateful to Manitoba Hydro for providing the facilities required for my experiments.

Thanks to my parents Mel and Anita, and my sister Chantelle for their support. After long days in the lab on weekends, it was nice to see them at family dinners. I appreciate

their interest in my work, but I had a lot of trouble explaining “partial discharge” to them without making them laugh.

I would like to thank my Pépère and Mémère, Roland and Yvette Jolicoeur for all of their support over the years. Both of them have taught me a lot in life. I would also like to acknowledge my late Baba and Gigi, Michael and Nell Partyka. They have made a huge impact on my character and they are missed dearly. Roland was an electronics technician at CN Rail before he retired and Michael was a math teacher. I am convinced that played a role in my career choice!

I would like to thank my friends and bandmates for putting up with my ludicrous schedule and enabling me to have some balance during busy times.

Finally, I would like to thank my wife, Rae-Ann, who woke up many weekend mornings to find that I was gone to work on my thesis. She has been very patient with me throughout this process and I could not have done this without her.

Dedication

To Baba and Gigi.

Table of Contents

List of Figures

List of Tables

Chapter 1

Introduction

This chapter will provide a description of the structure and function of large synchronous machines in addition to a detailed description of stator windings and an overview of partial discharge theory and measurement. This will help the reader associate specific defects in stator windings (discussed in Chapter 2) with partial discharge. Hydrogenerators will be the focus of this discussion since they have been studied most heavily by the author.

1.1 Problem Statement

Generator maintenance is valuable to utilities for two reasons: the generators themselves are expensive and time-consuming to build (and replace), and the cost of a forced outage can be high if the demand for electricity is high at the time. Therefore, measures should be taken to periodically assess the condition of the generators so any repairs or overhauls can be planned appropriately.

Over half of generator failures are a result of stator winding insulation failure [1]. There are many failure mechanisms of a stator winding, and most of them can be discovered by

detecting the presence of partial discharge [2]. Established methods exist for measuring partial discharge on stator windings, but little research is available on using antennas to measure stator winding partial discharge in the UHF range. In this thesis, antennas were designed and fabricated to perform partial discharge measurements on stator bars in the laboratory and on a stator winding at a generating station.

1.2 Hydrogenerator Structure and Function

Hydrogenerators are large synchronous machines that harness potential energy available from the difference in water elevations on either side of a dam (known as "head") to produce electricity. The flow of water from the forebay into the generator is controlled by wicket gates. Water spins a turbine connected to the rotor shaft and exits at the tailrace, which is at a lower elevation than the forebay.

A turbine or runner is connected to a shaft that spins at the synchronous speed which is the speed of the rotating magnetic field of the rotor [3]. This speed is held constant by the flow of water and a governor. Since the power frequency is fixed, an appropriate number of poles is selected to satisfy

$$n_s = \frac{120f}{P} \tag{1.1}$$

where n_s is the synchronous speed in rotations per minute (RPM), f is the frequency and P is the number of poles. Figure 1.1 provides a view of a turbine pit which lies directly beneath the rotor of a hydrogenerator.

A DC voltage (i.e. the "excitation") is applied to the rotor winding which induces a magnetic field. This rotating field propagates radially from the rotor across the air gap

Fig. 1.1: Turbine pit of a hydrogenerator.

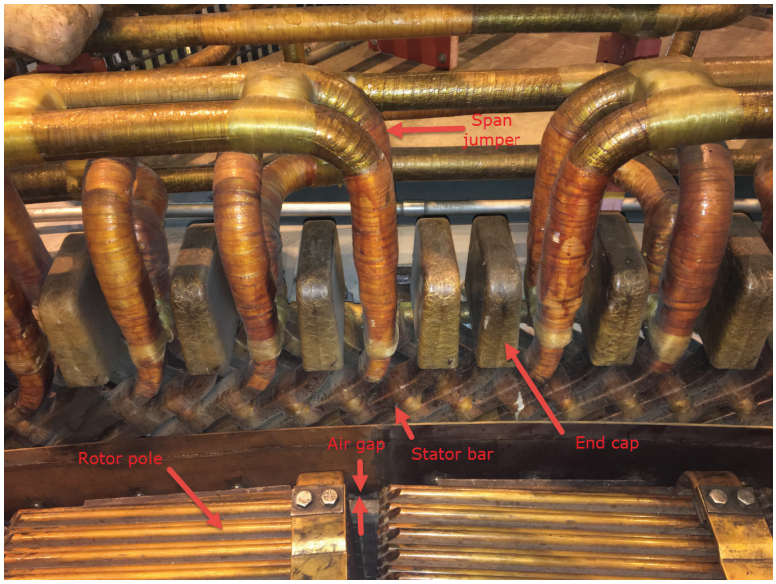

Fig. 1.2: Overhead view of rotor poles and stator of a hydrogenerator.

and into the stator core. Figure 1.2 provides an overhead view of rotor poles and a stator winding, showing the winding overhang region, end caps, and span jumpers. Note that the air gap is kept as small as possible to maximize the field produced in the stator.

The stator core is comprised of laminated sheets of steel to prevent the flow of axial currents, also known as eddy currents. Eddy currents create unnecessary losses and heating in the core steel [3]. The stator core has slots that house the stator winding. Even though the stator winding has a complex structure [2], it is effectively made up of multiple bars or coils formed from insulated copper and connected in series to form a phase circuit. Depending on the machine rating, there can be multiple parallel circuits per phase. The line end of the stator winding is connected to the generator output terminals, and the neutral end of the winding is typically connected to a grounding impedance. The magnetic field in the stator core induces a voltage in the winding which decreases linearly from the line to neutral end. The winding is arranged such that three voltages (or phases) are generated, each with the same magnitude but 120 electrical degrees apart. An overhead view of a generator with the rotor removed is shown in Fig. 1.3. A closer view of the same machine's winding is shown in Fig. 1.4 (note that stator wedges are missing in this figure).

Generator output terminals are connected to a step-up transformer by means of an isolated phase bus or cables (see Fig. 1.5). Important auxiliary assets are connected to this bus, but they are not discussed here as it is beyond the scope of this work [2, 3].

1.2.1 Stator Winding Construction

Low voltage motors and generators contain random-wound stator windings which are made from insulated wire that is looped in the slots to form a coil [2]. Windings rated above 2300 V (including hydrogenerators) are made with form-wound coils or Roebel bars [1].

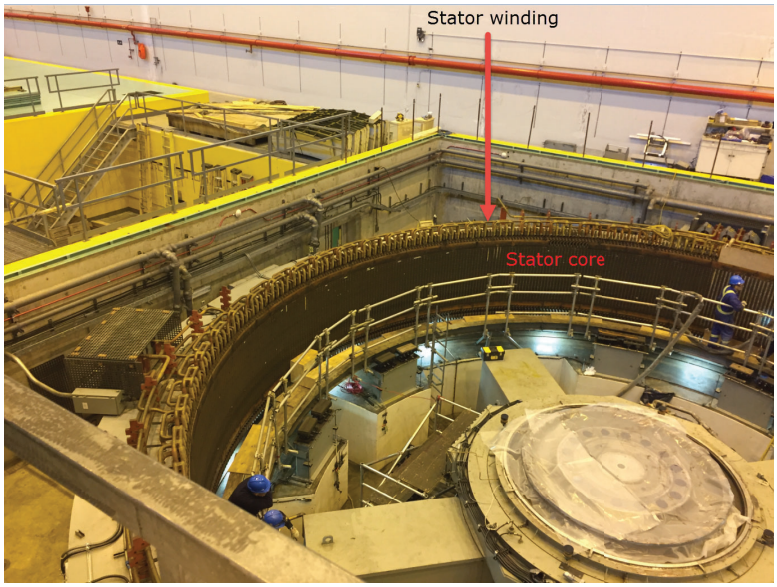

Fig. 1.3: Overhead view of a hydrogenerator with the rotor removed.

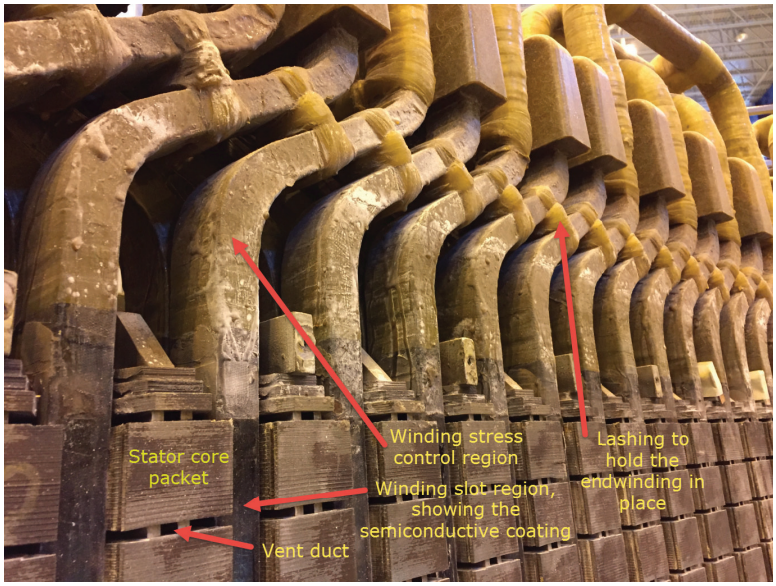

Fig. 1.4: Close-up view of the top of a stator with wedges removed.

Fig. 1.5: Stator terminals (bottom) and isolated phase bus terminals (top). They are connected in-service.

Form-wound coils are manufactured in a factory and are made to fit inside the stator slots. Turn insulation separates each turn within a coil. Roebel bars are half-turn coils that are made with conductors that are transposed at various points along the length of the bar to reduce eddy currents and circulating currents in the copper [2]. They are used in high power machines (typically above 75 MW) and are easier to install than coils. This thesis will focus on form-wound coils and bars since random wound coils are not found in high voltage rotating machines which are prone to partial discharge. Figure 1.6 shows a cross-section of a coil with four turns, showing various components of the insulation system. High voltage conductors are comprised of multiple strands to increase current-carrying capacity and to reduce eddy currents. Voltage between strands is very low (less than 10 V) and therefore strand insulation is typically a glass insulation specified for increased mechanical strength for the roebelling process. Turn insulation in multi-turn coils is required to prevent turn

shorts, which can cause permanent damage to a stator in a matter of seconds [1]. Turn insulation operates at a higher temperature than groundwall insulation since it is closer to the conductors. It is comprised of mica paper with glass backing and is sometimes combined with the strand insulation [1]. Roebel bars do not have turn insulation as they make up half of a single turn. Groundwall insulation prevents shorts between conductors and the grounded stator core. Generally, groundwall insulation is comprised of layers of mica tape impregnated with resin. Older windings contained thermoplastic materials in their resins such as asphalt, but modern windings use thermoset materials such as epoxy or polyester.

After the winding insulation is formed, windings are cured in an oven until the optimal dielectric properties of the insulation are attained [1,2]. Once the stator coils/bars are cured, a semiconductive coating (or tape) is applied around the groundwall insulation in the slot portion to evenly distribute the electric field. To avoid localized electric fields in the slot exit regions of bars and coils, a stress control coating with nonlinear resistive properties (such as silicon carbide) is applied to a specific region of the endwinding (according to the manufacturer's specification). Bars/coils are then placed into the stator slots. Brazed connections are made to connect the individual bars/coils and then the winding is wedged in place to limit the effects of vibration. Figure 1.7 shows the external components of a coil's insulation system. The coil has been placed in a dummy slot that simulates a real stator slot.

1.3 Partial Discharge Overview

Partial Discharge (PD) is the partial electrical breakdown of high voltage insulation [4]. PD can occur within solid insulation systems that contain defects such as air pockets, voids,

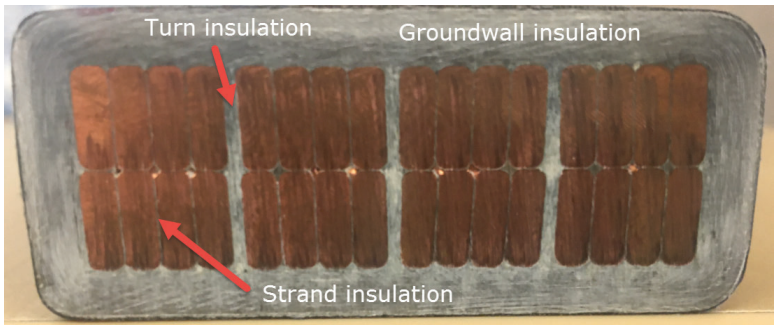

Fig. 1.6: Insulation within a four-turn coil of a large hydrogenerator.

water trees (in cables), or contamination. In liquid insulation, like that found within an oil-filled transformer, PD can occur in the presence of air bubbles. PD can also occur on insulation surfaces where the electric field density is high enough to ionize the surrounding materials due to poor design or installation, physical damage, or contamination. PD in the surrounding air of a high voltage conductor is referred to as corona [4]. Even though PD originates from the insulation system, this does not mean that the insulation quality is necessarily poor and requires replacement. PD can be a symptom of other issues such as mechanical damage, contamination, excessive vibration, buckling due to thermal cycling, etc. Over time, the PD itself or the root cause of the PD can lead to equipment failure. PD can help detect manufacturing defects or poor workmanship during the installation of various assets. This is why PD tests are performed on many different types of assets at the manufacturing, installation, commissioning, and maintenance phases of an asset's life cycle.

While there are different types of partial discharge events such as pulse-type, pulseless glow and pseudoglow discharges, research and development in the field of PD measurement has almost exclusively focused on pulse-type discharges [5]. In a pulse-type partial discharge event, applied voltage exceeds the breakdown voltage of the cavity, causing electrons to

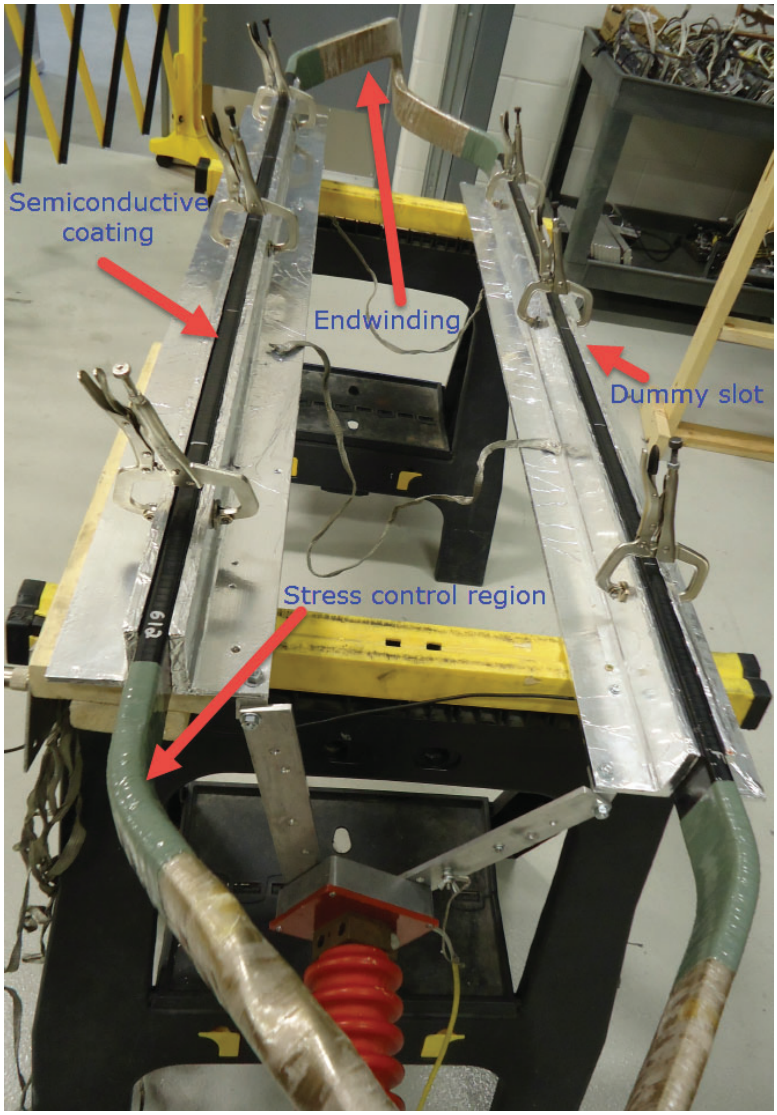

Fig. 1.7: A coil in a laboratory with its external components labeled.

rapidly travel across it. This electron avalanche creates a high frequency current pulse in the insulation, with characteristics dependent on insulation materials, applied voltage, and cavity temperature, pressure and geometry. Slower ionic movement incites a small current that persists longer than the initial electron avalanche [1].

1.3.1 Measurement of PD Pulses

After a PD event occurs in an insulation system, the resulting current pulse will propagate to the high voltage conductor and travel in both directions. The most common way to measure PD is to measure the PD current pulse with the use of a coupling capacitor, with one terminal connected to the specimen's high voltage bus and the other terminal connected to a measurement impedance [4, 6, 7].

Figure 1.8 shows a typical high voltage PD test circuit. The variable autotransformer allows the user to achieve precise test voltages, and it also helps to determine the PD inception voltage (PDIV) and PD extinction voltage (PDEV). The test transformer is required to step up the voltage since conventional voltage sources and variable autotransformers are not rated for high voltage. The insulation in Fig. 1.8 is modeled by a lumped capacitor which is sufficient for practical applications, but it is not totally accurate since leakage, contamination, and material non-uniformity will create a complex RC network. Capacitance bridge measurements have revealed that while steady state current through insulation is mostly capacitive, it does indeed have a small resistive component [8].

On a rotating machine, coupling capacitors can be connected to the circuit ring bus (on large machines), the machine terminals, or the isolated phase bus [1]. Capacitive couplers can also be placed in end caps, or fabricated with cables cut to a specific length. The coupling capacitance and measurement impedance serve as a high pass filter, allowing high frequency

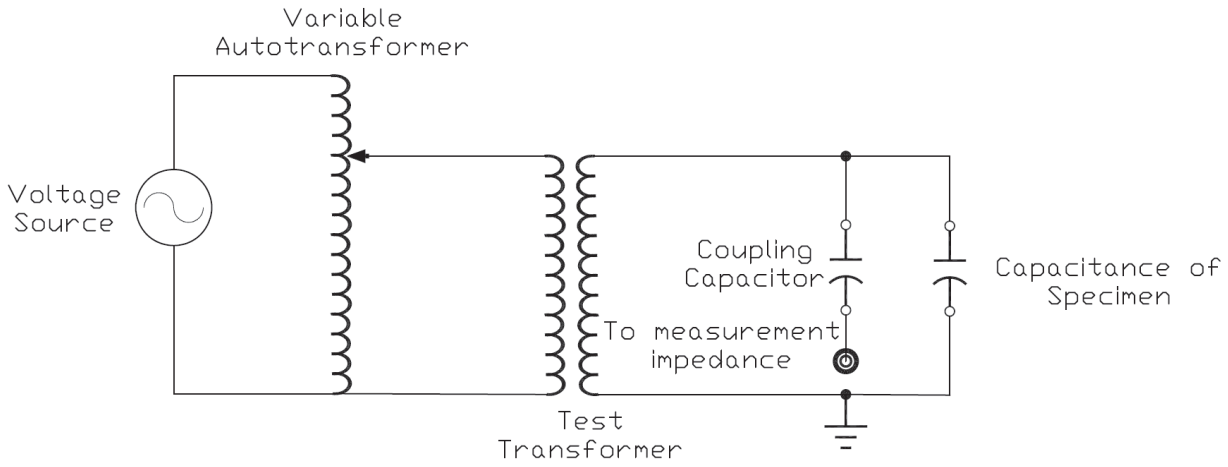

Fig. 1.8: Simplified high voltage setup for PD measurement in a laboratory.

PD pulses to be measured while reducing the 60 Hz component at the coupler output to voltages typically under 10 V. See Fig. 1.9 for a photo taken during the installation of 80 pF coupling capacitors on a new stator winding. Note that these couplers are not yet connected to the leads which are attached to the ring bus.

While PD events are commonly detected by measuring the electric current, they can also be detected by measuring acoustic signals, ultraviolet signals, radiated electromagnetic fields, and chemicals. Commercial systems exist that use ultrasonic triangulation to determine the location of PD inside a transformer tank [9]. Corona can be visually recorded on a test specimen with the naked eye (by seeing sparking for example) or with the use of a UV camera or acoustic sensor. Chemicals produced during the PD event such as ozone can be detected. Electromagnetic fields that are radiated from PD pulse currents can be detected wirelessly with the use of a near field capacitive sensor or an antenna. PD can also be measured using the currents induced by the radiated fields in an HFCT winding [4].

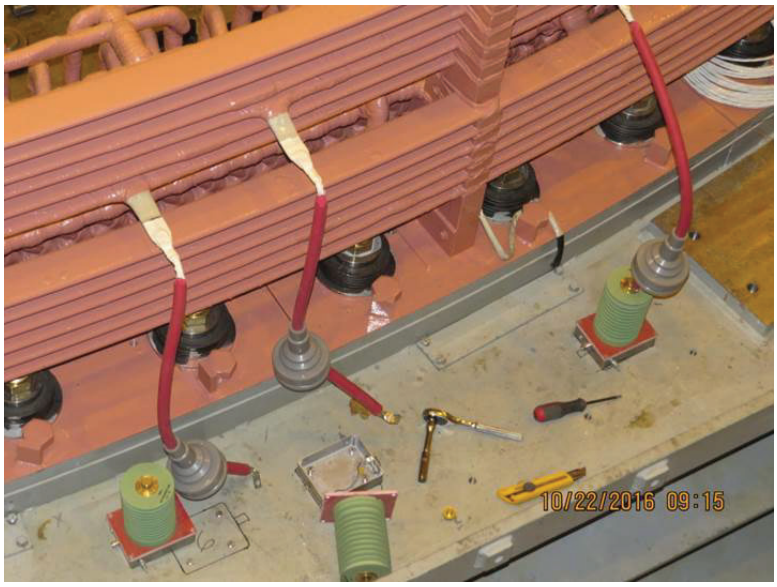

Fig. 1.9: 80 pF coupling capacitors being installed on the circuit ring bus of a large hydrogenerator. The coupling capacitors are not yet connected.

1.3.2 PD Data Analysis

PD measurement systems are capable of detecting thousands of pulses per second. As it is not practical for users to analyze every waveform individually, several methods exist which help to present the PD data in a useful manner. For example, it is typical to record the peak magnitude of each PD pulse, along with polarity and phase location (relative to the power frequency cycle). Statistics such as a weighted average can be calculated with aggregate peak magnitude data. This helps to provide a PD magnitude representative of all the acquired pulses. It is common to plot the peak of each PD pulse magnitude against power frequency phase [6]. This plot is known as a Phase Resolved Partial Discharge (PRPD) pattern. Pulse phase location can be used to determine whether the measured PD activity is internal or external to the insulation system by knowledge of the fact that PD close to the conductor

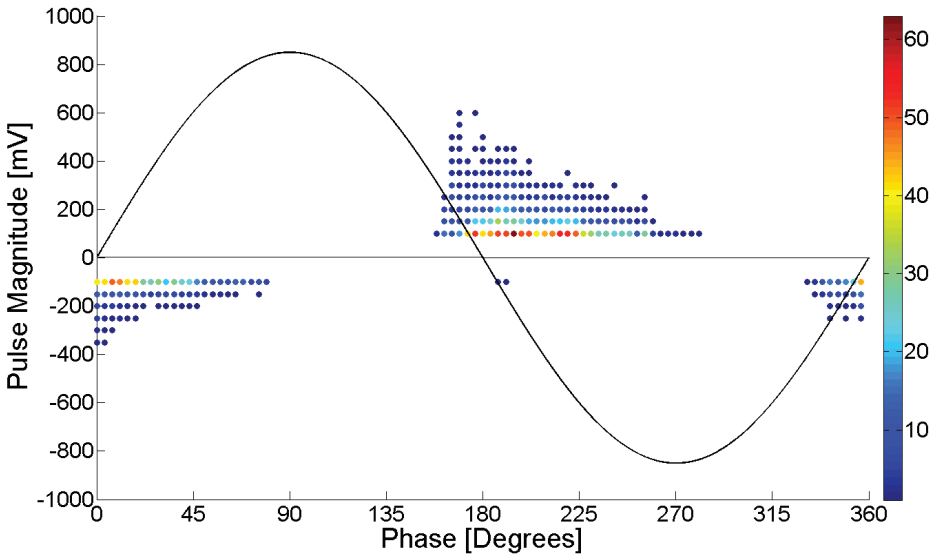

Fig. 1.10: PRPD pattern from an online measurement performed on a hydrogenerator, showing slot discharge.

has predominance in the positive half cycle and PD on the surface has predominance in the negative half cycle. It can also show evidence of noise and disturbances such as thyristor pulses in a High Voltage Direct Current (HVDC) converter station. Pulse phase location and shape of the plotted pulse clusters can be used to diagnose specific insulation defects in rotating machine windings. IEC 60034-27-2 provides examples of PRPD patterns and their associated defects [7]. Figure 1.10 was produced from an online PD acquisition with a commercial instrument on a hydrogenerator winding. An 80 pF coupling capacitor was installed on the generator's ring bus to detect PD. In the figure, the colour gradient represents the total amount of pulses in a five second window. This was done to be consistent with other PRPD patterns in this thesis, but normally the colour bar would represent a repetition rate. This plot agrees with the example of slot discharge activity as shown in IEC 60034-27-2 [7].

Another common plot used for rotating machine PD data analysis is the Pulse Height Analysis (PHA) plot. In this semilog plot, PD magnitude is plotted against repetition rate (i.e. pulses per second). Two curves are included; one for positive pulses and another for negative pulses. Figure 1.11 is the PHA plot associated with the PRPD pattern depicted in Fig. 1.10. Partial discharge pulse polarity predominance is another metric that can help pinpoint issues in the insulation system [7]. In North America, negative pulses correspond to issues near the conductor and positive pulses correspond to issues on the insulation surface. Outside North America, the definition of a positive and negative PD pulse are often reversed. Quantities described in IEEE 1434 can be derived from the PHA plot, such as Qm and Normalized Quantity Number (NQN) [4]. Qm is the PD magnitude corresponding to a specific pulse repetition rate (10 pulses per second is used in this thesis) and NQN represents the normalized area under a PHA plot curve. It is more common to quantify rotating machine PD measurements in terms of Qm.

Other plots can be generated to help analyze PD data. Using convolution methods, time frequency maps can be generated which can be used to discriminate PD signal sources in the PRPD pattern [7] [10]. Measurement systems that perform simultaneous three-phase PD measurements on rotating machines can generate a three-phase, three-dimensional PRPD pattern [11].

1.3.3 Measurement Bandwidth

PD pulses contain frequency content from DC into the UHF range [7]. IEC 60270 provides guidelines for bandwidth that enables measurements to be repeatable [6]. As per the standard, the lower frequency limit can range from 30-100 kHz, the upper frequency limit must be equal or lower than 1 MHz, and the total bandwidth must range between 100 and 900

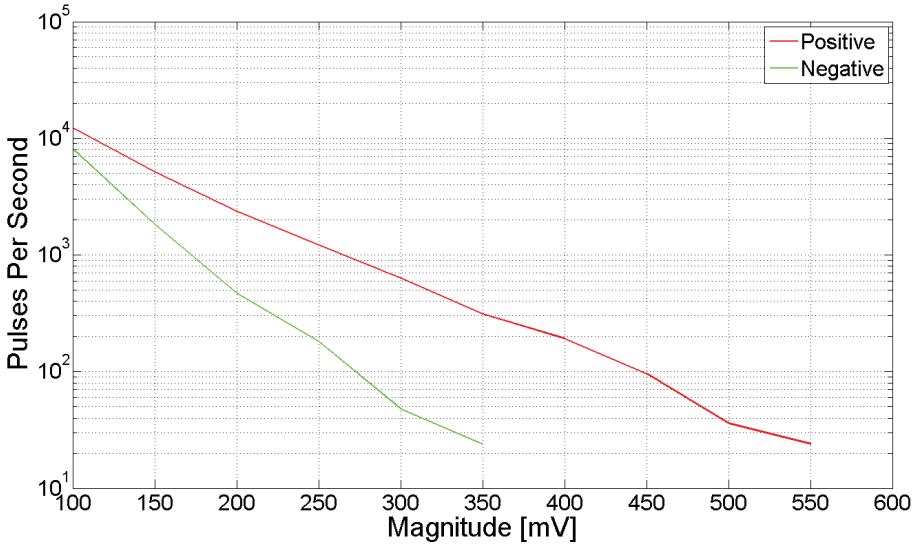

Fig. 1.11: PHA plot associated with PRPD pattern in Fig. 1.10.

kHz. These guidelines are not always practical, especially in a station environment where noise is very high at these frequencies. For PD measurements on rotating machines in the field, higher bandwidths (in the VHF range or higher) are required to achieve an acceptable signal to noise ratio [7].

1.3.4 Calibration

To accurately measure the PD magnitude, IEC 60270 provides guidelines for calibrating the apparent charge which is the charge that provides the same reading on the measuring instrument as the PD current pulse when injected within a very short time between the specimen's terminals. This is done by injecting a known charge into the test specimen, measuring the response, and calculating a scale factor to ensure charge measurements during the actual test are accurate [6].

In stator windings, pulse attenuation and dispersion, resonance, and cross-coupling betweeen phases make calibration impossible. Therefore, rotating machine PD is typically measured in units of voltage instead of charge. IEC 60034-27-2 recommends a sensitivity check which involves injecting a known charge and measuring the response at the PD coupler's output [7]. Even though it is the norm to record PD in units of voltage on rotating machines, efforts have been made to measure PD in units of charge [11].

1.4 Motivation

PD is a quantity that can be used to assess the condition of a rotating machine's insulation system. It can expose serious issues in stator winding insulation which, if corrected before failure, can prevent costly forced outages. An example of such a failure can be seen in Fig. 1.12 and Fig. 1.13. To describe this failure event, two coil turns shorted together which created extremely high currents and heating, causing the copper to melt and build pressure inside the coil. Eventually, there was a ground fault and the molten copper exploded, exiting at the rear of the stator. Fragments of copper could be found all over the rear of the stator, and the surrounding areas were severely charred by the heat. Luckily, the stator core was not damaged, otherwise the generator would have been out of service for months instead of weeks. Improvements in PD measurement techniques might have the potential to prevent similar failures in the future.

Online PD measurements are performed by many machine owners, but as will be discussed in Chapter 2, most users employ VHF techniques with capacitive couplers or UHF techniques with near-field sensors. There is some research on the use of antennas to measure radiated PD in the UHF range, but there is little research on the application to online

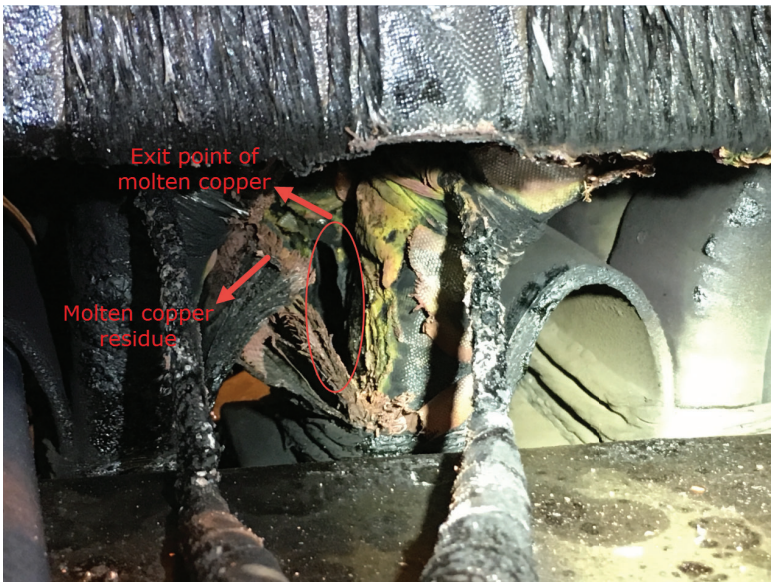

Fig. 1.12: Rear view of failed coil that experienced a turn to turn fault.

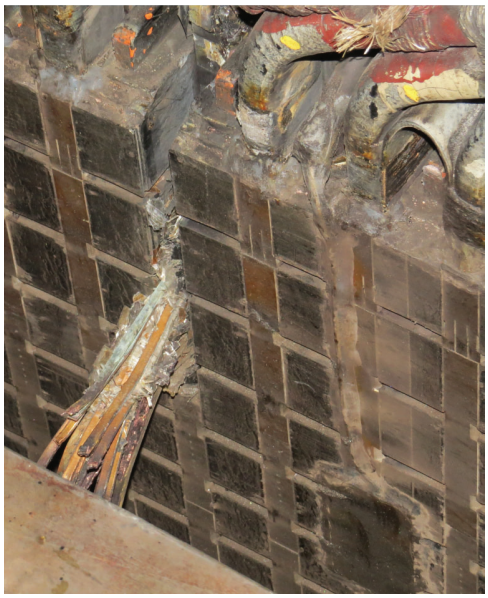

Fig. 1.13: Front view of failed coil that experienced a turn to turn fault.

rotating machines. In addition, no PRPD patterns created from PD acquired with UHF antennas have been found in the literature. Since antennas are easy to install and have good noise immunity in a station environment, they may have the ability to complement existing sensors used in the industry.

1.5 Objectives of the Thesis

The goal of this thesis is to investigate the viability of online stator winding PD measurements using UHF antennas. Specific objectives include:

- Design and fabricate UHF antennas that are appropriate for detection of PD and feasible for use in a rotating machine.
- Once antennas are designed and fabricated, verify their performance and response to PD.
- Develop a method of acquiring PD pulses with antennas and generating PRPD patterns.
- Perform high voltage PD measurements on single bars and/or coils in a laboratory setting.
- Perform online PD measurements on a hydrogenerator.
- Compare results with data acquired from a commercial measurement system.

1.6 Research Contributions

The contributions of this thesis are as follows:

- Analysis of PD experiments with UHF antennas placed in the far field.
- Evaluation of UHF antenna-based techniques for PD measurement on stator bars in a laboratory setting.
- Evaluation of UHF antenna-based techniques for PD measurement on the winding of an operational hydrogenerator.
- Analysis of PRPD patterns obtained with UHF antennas.

1.6.1 Publications

In June 2019, a conference paper was presented at the IEEE Electrical Insulation Conference which was held in Calgary, AB [12]. The paper was entitled "UHF Measurement of Partial Discharge on Stator Bars Using Patch Antennas."

Chapter 2
Literature Review

2.1 Types of Stator Winding PD

The manufacturing process of stator windings results in the formation of microvoids (or small air pockets) in the groundwall insulation. Due to this, it is normal to measure some PD in healthy windings [7]. Windings are able to withstand a base level of microvoid PD because mica is inherently PD-resistant. Other types of PD in stator windings are listed below and described based on the literature [1, 2, 4, 7]:

- Discharge between mica tape layers due to delamination (tape separation) can occur within the groundwall insulation due to manufacturing defects or thermal/mechanical stress. Delamination can also occur between the groundwall insulation and copper conductors due to thermal cycling which can cause PD.
- Slot discharge occurs when the semiconductive coating around the winding is compromised, resulting in discharges between the winding surface and the grounded stator core.

- Discharge in the stress control region occurs when the stress control coating is degraded and localized electric fields create PD on the winding surface at the slot exit.
- Endwinding discharges can occur due to contamination (including dirt and metallic particles), the formation of conductive paths (tracking), and poor clearances between phases in the winding overhang region.
- Arcing can occur due to poor connections at the flexible links in the winding terminals. It can also manifest due to vibration sparking; a phenomenon where vibration causes arcing between the winding surface and the grounded stator core.

2.2 Challenges of Measuring PD in the Field

2.2.1 Propagation of PD Pulses in Stator Windings

The most widely understood mode of PD pulse propagation in stator windings is the transmission line mode [1]. In this mode, the avalanche of electrons in a partial discharge event produces a current pulse in the insulation with a rise time of less than 5 ns. This pulse propagates to the winding conductor and travels in both directions along the length of the stator winding. The stator winding structure behaves as a transmission line and as such, the PD pulse is attenuated and dispersed along the length of the winding [7]. Therefore, the measured PD waveforms do not represent the charge at the actual PD site within the insulation. In addition, there are resonances in the winding due to internal inductance and capacitance, and also cross-talk from other phases due to capacitive coupling of PD in the endwindings [1, 13]. These attributes make it challenging to quantify PD activity. Due to pulse attenuation, PD measurement systems for rotating machines (that use the electrical

pulse method) are typically only capable of measuring pulses in 10-15% of the winding closest to the PD sensor [14]. Since winding voltage decreases linearly from the line to neutral end, most PD should occur at the line end. This is where PD sensors are installed.

2.2.2 Noise and Disturbances in Rotating Machine PD Measurements

In high voltage laboratories, specific shielding and grounding schemes allow the detection of PD pulses with low apparent charge (2 pC in Manitoba Hydro's High Voltage Test Facility). In a powerhouse, stator winding PD detection is made complicated by the abundance of noise and disturbances. Some examples of disturbances include communication signals, power line carrier signals, and switching pulses (originating from voltage rectifiers such as static exciters or thyristors in an HVDC converter station). Work activities nearby such as craning or welding can introduce interfering currents through station grounds that can be detected by PD sensors. High frequency signals can couple to the isolated phase bus from many locations in the station and propagate to the winding terminals.

Due to the high level of noise and disturbances in station environments, conventional wideband measurements as per IEC 60270 are not used for measuring stator winding PD. Noise level decreases with increasing frequency, and this is why commercial systems typically perform measurements in the VHF range. Even in the VHF range, noise is still an issue [7]. Therefore, noise cancellation techniques are required to eliminate signals external to the winding [1, 11].

2.3 Typical Winding PD Measurement Methods

Owners of rotating machines have been performing online PD measurements for decades and various commercial systems are available [11, 15–17]. One popular PD measurement system uses 80 pF coupling capacitors to measure PD current pulses in the VHF range, from 40 to 350 MHz [1, 18]. To overcome noise issues described above, two couplers are installed and time-of-arrival methods are implemented to cancel noise. For machines that have a circuit ring bus length greater than 2 m, couplers can be installed on the ring bus and a differential technique can be used to eliminate noise. On smaller machines, one coupler can be installed at the machine terminals, and the other coupler can be installed further along the isolated phase bus. Noise cancellation is achieved using a directional method, which requires knowledge of the electrical distance between each coupler. In order to measure PD on all phases, at least six couplers are required using above methods. This number can increase if it is desired to perform differential measurements on all stator circuits. There are continuous online measurement systems that use similar coupling capacitors as described above, but noise cancellation is based on simultaneous three-phase measurements [11]. Therefore, only three capacitors are required to detect PD on all three phases.

Other measurement schemes are detailed in IEEE 1434. They include the use of CTs, surge capacitors, stator slot couplers, and antennae to detect PD [4].

2.3.1 Stator Slot Couplers

The Stator Slot Coupler (SSC) is an online PD sensor used exclusively for rotating machine windings [19]. While capacitive couplers are more widely used than SSCs, there were at least 1000 machines known to be equipped with SSCs in 2013 [18]. The SSC, shown in Fig. 2.1,

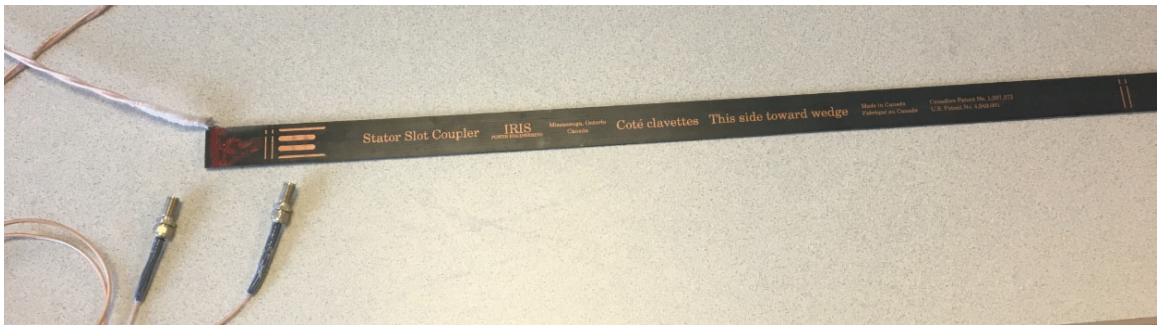

Fig. 2.1: Photo of a stator slot coupler manufactured by IRIS Power.

is a sensor that is designed to be installed on top of a bar or coil, underneath the wedge in a stator slot [20]. The wedge-facing side of the SSC is a ground plane. The other side (facing the bar/coil) contains a 45 cm, 50 Ω trace with an FR-4 substrate. Proximal high frequency PD currents are coupled to the trace. Both ends of the trace are connected to RG178 cables of the same length that exit at the endwinding side of the sensor. Both cables are terminated with 50 Ω at the measurement device, which allows discrimination between pulses originating from the end arms and pulses originating further into the slot. Noise is eliminated based on pulse shape, specifically by virtue of the fact that noise is oscillatory and longer in duration than PD [20, 21]. SSCs were designed to detect pulses with rise-times of 1-3 ns [20]. It has been shown that on large turbine generators, SSCs have better noise immunity than capacitive couplers due to the higher frequency range used for measurement [18].

In order to better understand SSCs, experiments were performed on a spare SSC available to the author. First, the scattering or "S" parameters of the SSC were measured. Scattering parameters are used to describe N-port microwave networks in terms of incident and reflected voltage waves. The scattering parameters for any n-port network can be calculated using [22]

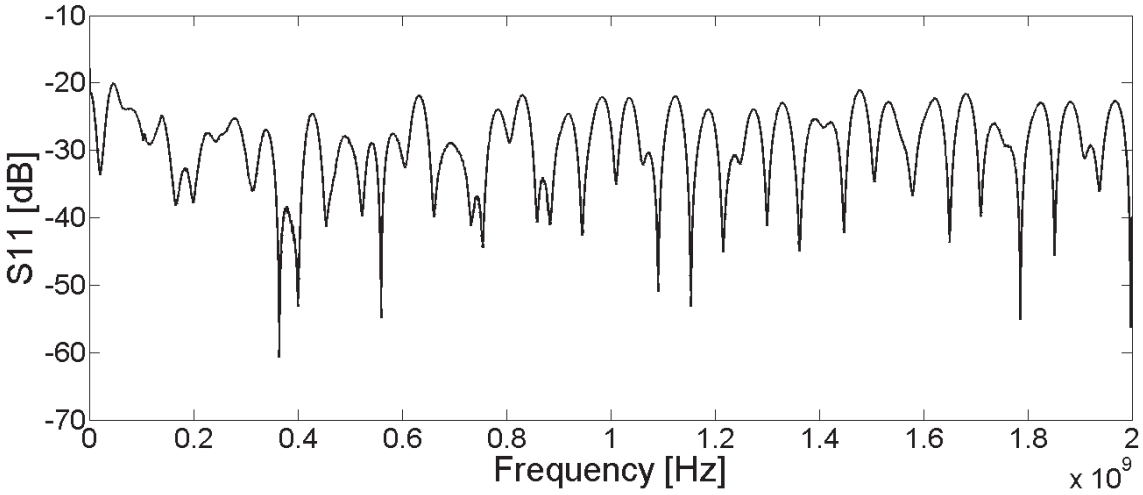

Fig. 2.2: S_{11} of a stator slot coupler.

$$S_{ij} = \frac{V_i^-}{V_j^+}, V_k^+ = 0 \quad \text{for} \quad k \neq j \tag{2.1}$$

where V_i^- is the measured voltage wave from the specimen at port i, and V_j^+ is the incident voltage wave at port j. Applying (2.1) and the theory in [22], the SSC is considered as a two-port network with a 2×2 scattering matrix. To measure the scattering parameters, the SSC cables were connected to a Vector Network Analyzer (VNA)[1]. The endwinding cable was connected to port 1 and the slot cable was connected to port 2. S_{11} of the SSC (shown in Fig. 2.2) was less than -20 dB up to 2 GHz. S_{11} is a measure of the reflected wave returning to the source, so this indicates that the SSC is matched well to 50 Ω. The S_{21} plot (shown in Fig. 2.3) indicates that the the sensor behaves as a lossy transmission line. This sensor has been called a UHF antenna in some publications [18], but it is rather a transmission line with a stripline structure.

[1]Keysight E5063A VNA 100 kHz - 8.5 GHz

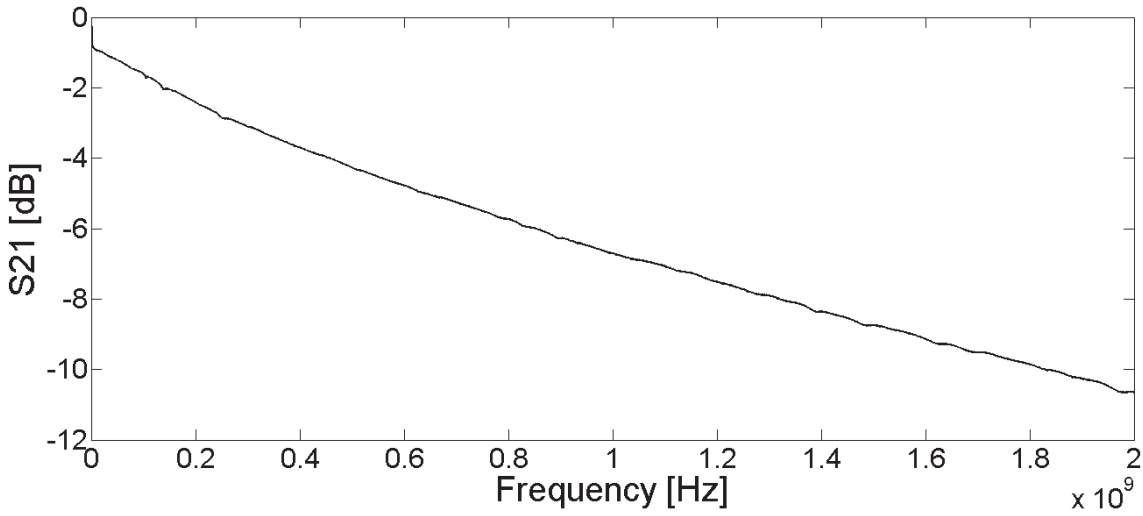

Fig. 2.3: S_{21} of a stator slot coupler.

Other experiments were performed with an impulse generator that produces pulses with a 370-ps rise-time. Figure 2.4 shows this pulse injected into the 1 MΩ input of an oscilloscope. Note that the pulse was not injected into 50 Ω due to the possibility of damaging the oscilloscope channel by exceeding its voltage limit. As a result, reflections of the pulse can be seen in the figure.

The impulse was injected into a parallel plate assembly with the SSC placed in between the plates. The goal of this experiment was to mimic PD pulses at various locations along the SSC's length, simulating pulses occurring in a real stator slot. Figures 2.5, 2.6, and 2.7 show SSC response with the parallel plate assembly held near the endwinding, slot, and middle portions of the SSC respectively. This experiment verified the sensor's response as described by the literature [20] and as predicted by the S-parameter measurements.

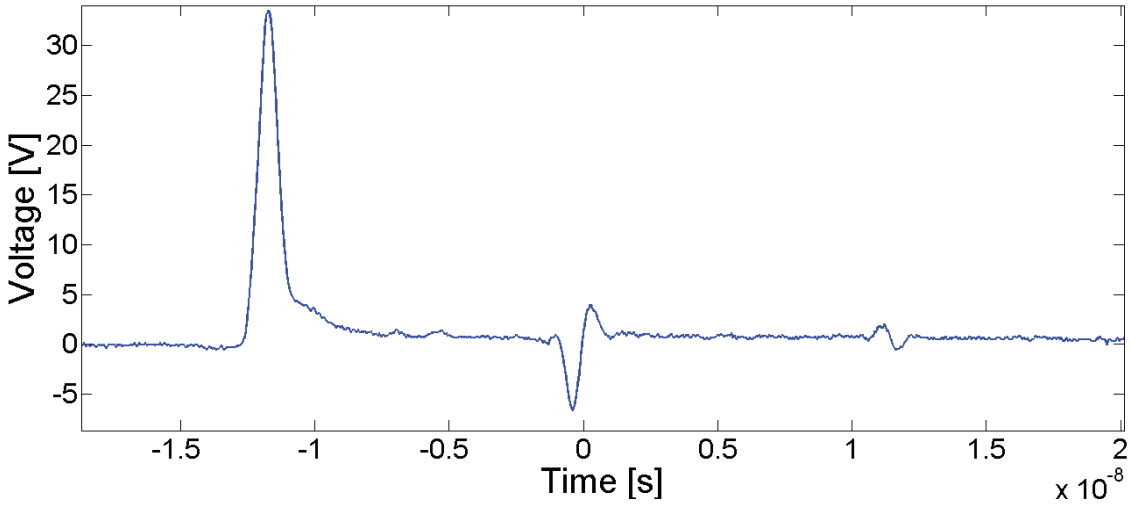

Fig. 2.4: Pulse with 370ps rise-time terminated into 1 MΩ at the oscilloscope.

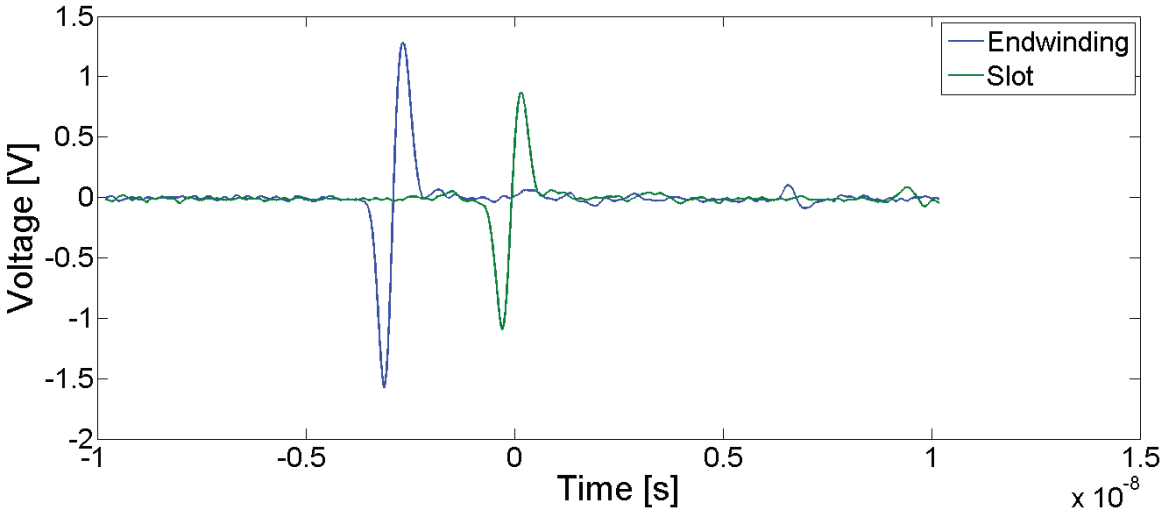

Fig. 2.5: SSC response to impulse injection near endwinding region.

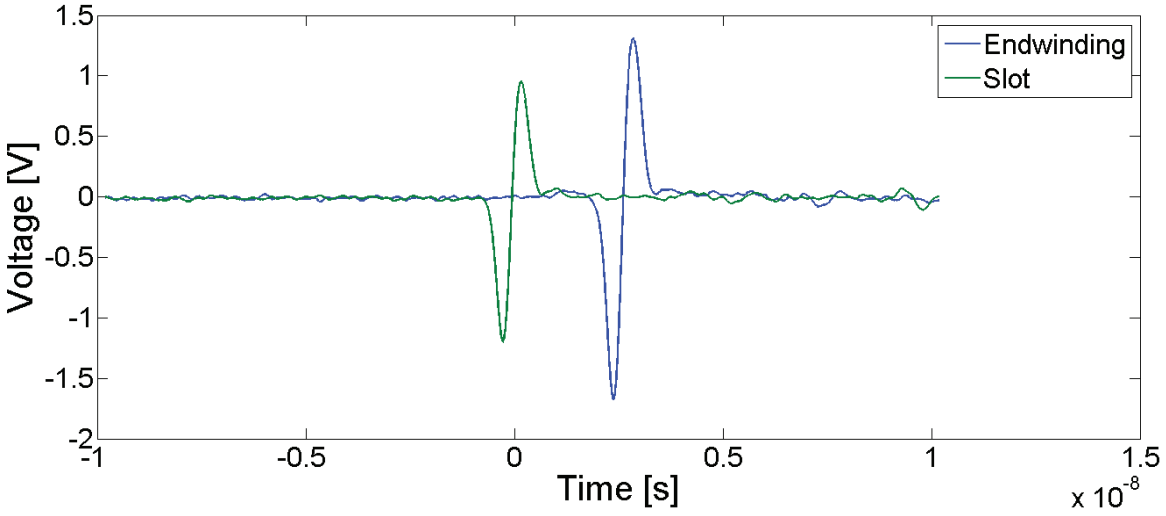

Fig. 2.6: SSC response to impulse injection near slot region.

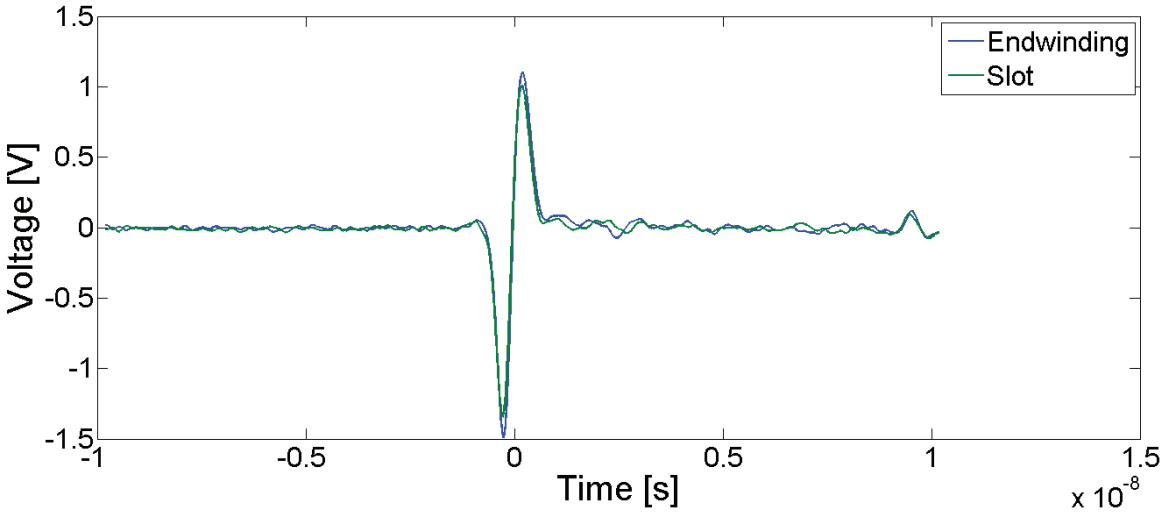

Fig. 2.7: SSC response to impulse injection near the middle of the SSC.

2.3.2 TVA Probe

In the 1960s, an electromagnetic sensor was developed by Tennessee Valley Authority (TVA) to measure offline PD on stator windings [23]. As such, this sensor is commonly called the "TVA Probe." It is effectively an antenna made from wire wrapped around a ferrite core. The antenna is tuned to 5 MHz and is fed to a peak current detection circuit. To perform PD measurements with this sensor, the machine is taken offline, and the rated line-to-ground voltage is applied to the winding using an external voltage source. The probe is then pressed against the stator wedge in each slot (in various locations if desired) and the peak current is recorded [4]. Since a reading can be obtained for each slot, this sensor can help localize issues in the winding. After decades of experience with this sensor, maximum current limits have been recommended in [4] for different insulation types. Figure 2.8 shows a portion of the stator face on a hydrogenerator. In the figure, rotor poles are removed for stator wedge inspections but typically they are in place. This makes TVA probe measurements only possible at the top of each slot.

2.4 Antennas for PD Measurement

Both sensors discussed in the previous sections do not operate as antennas because they are placed in the near field. As proof of this, we can use three field regions that were derived in [24] based on the model of a thin dipole antenna with finite length. The reactive near-field, Fresnel, and far-field regions are defined in

$$0 < r < 0.62\sqrt{\frac{D^3}{\lambda}}, \tag{2.2}$$

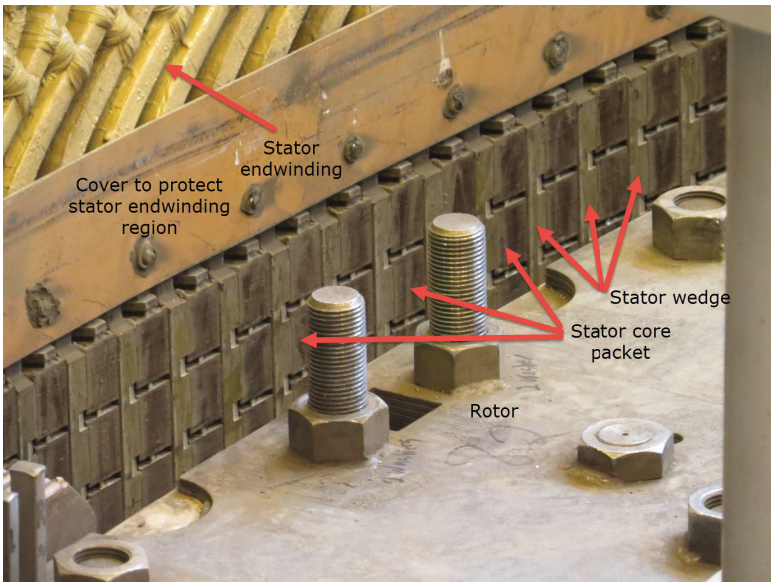

Fig. 2.8: View of the top of an epoxy mica stator winding of a hydrogenerator with the rotor in place but with poles removed.

$$0.62\sqrt{\frac{D^3}{\lambda}} \leq r < \frac{2D^2}{\lambda}, \tag{2.3}$$

and

$$\frac{2D^2}{\lambda} \leq r \tag{2.4}$$

where λ is the wavelength, D is the largest dimension of the antenna, and r is the distance from any point on the antenna to an observation point. It should be noted that (2.4) generally applies to large antennas (arrays). If the size of an antenna is less than $\frac{\lambda}{2}$ (such as a single element patch antenna), the far field region is usually considered to be where $r > 5\lambda$. Both sensors discussed above are in the reactive near field as they are only millimetres away from the stator winding.

Research was conducted to evaluate which antennas are being used or studied for PD measurements [25–33]. The investigation included antennas designed for PD measurement on various assets (not only rotating machines), but antennas designed specifically for power transformers and gas insulated switchgear (GIS) were ignored. All antennas in the research were used in conjunction with signal conditioning systems which included some form of amplification and filtration. The research is summarized below:

a. A 250 MHz commercial wideband log periodic antenna was used to measure PD in a medium voltage cable by placing the antenna near both cable terminations. PRPD patterns and time frequency maps were compared to those obtained with an HFCT placed on the sheath ground at each end of the cable. The PRPD patterns showed some agreement between both sensors [25].

b. A Hilbert antenna was designed for PD detection due to its wideband properties and small size. The antenna was designed to capture PD activity from 300 to 3,000 MHz. It was determined that a third order Hilbert antenna performed best, based on return loss (S_{11}) simulations in [26]. The resonant frequencies of this antenna were 960 MHz, 1.78 GHz, and 2.50 GHz [26].

c. A modified bowtie antenna was designed and fabricated to measure PD at 1,500 MHz. Return loss measurements were performed and compared to simulations. Needle plane measurements were performed with the antenna placed 10 cm away. The antenna did respond to PD in the needle plane jig [27].

d. Needle plane measurements were made with a loop antenna. The antenna was moved further and further away from the needle plane jig until the response became equal to the background noise level. This distance was 2.25 metres. The bandwidth of the

antenna was not specified in the research, however it is said to operate in the UHF range [28].

e. A monopole antenna with a measurement system bandwidth of 120-900 MHz was used to measure PD from a sphere gap and a 40 mm air gap. With a 19.2 kV voltage applied to the air gap, PD was measured up to 4 m away [29].

f. PD was measured with a 10 cm spherical probe on individual stator coils. The sensor has a non-resonant response from 0.1-100 MHz. It was placed at various locations in the end arm regions. PD was confirmed on this coil with UV detection near the stress control/semiconductive coating interface. The most sensitive measurement was 40-50 cm away from the coil, which corresponds to the radiated near field [30].

g. Researchers have investigated the use of D-Dot sensors for PD detection. A D-dot sensor measures a voltage that is proportional to the rate of change of the electric displacement vector. In order to retrieve the original voltage signal from the D-dot sensor, an integrator must be used. A possible advantage of this sensor for PD detection is that due to its ability to respond to low voltages, an external power frequency reference voltage input may not be required for PRPD pattern creation [31]. There has been research on D-dot sensors for PD measurement in switchgear [32], but noise has been cited as a severe problem [33].

2.4.1 Microstrip Patch Antenna

A commercial measurement system using microstrip patch antennas was developed based on research from the 1990s [34–36]. The research claims to have measured PD on an offline generator using two antennas and applying a spatial phase difference method to eliminate

noise. Developers of the commercial system chose a center frequency of 1.8 GHz because they found that ambient noise was reduced at frequencies above 1.5 GHz at a local power plant [37]. The interaction of the electromagnetic fields radiated by the PD pulses and a microstrip patch antenna is described in [38] using a dipole model as the PD source.

Other researchers used a 900 MHz patch antenna to study response waveforms, the effect of antenna distance from the PD source, and the PD intensity versus applied voltage [39]. As expected, the PD intensity increased with the applied voltage and decreased with the distance of the antenna [39].

A microstrip patch antenna with a center frequency of 450 MHz was designed and it was reported that there was a response up to 15 m away during needle plane measurements [40]. Researchers chose to investigate the use of antennas due to the simplicity of installation compared to other methods of detection [40].

Another microstrip patch antenna was designed with a centre frequency of 500 MHz. In this research, PD pulse waveforms were studied, antenna radiation patterns were provided, and the effect of the distance of the antenna was studied from needle plane PD measurements. The patch antenna was chosen because it is simple, lightweight, and mechanically robust [41].

2.5 Conclusions from Literature Review

After reviewing the literature, the following conclusions can be made:

- The most common way to measure PD on rotating machine windings is with coupling capacitors in the VHF range.
- Stator slot couplers are able to measure online stator winding PD in the UHF range wirelessly by coupling capacitive currents from nearby stator bars/coils.

- The microstrip patch antenna is the most prevalent UHF antenna for stator winding PD research. Additionally, the microstrip patch antenna is the only UHF antenna that is used in a commercial measurement system.
- Selection of bandwidth generally appears to be arbitrary.
- Installation of UHF antennas for PD measurements does not necessarily require an outage. This is in contrast to coupling capacitors and stator slot couplers which require physical modifications of the stator prior to installation.

Research on stator winding PRPD patterns obtained using UHF antennas has not been found. In addition, there is a lack of analysis of the optimal frequency band to use in the UHF range and there is little objective reasoning for antenna selection.

It has been shown, however, that PD detection is possible in the UHF range. The rest of this thesis will focus on PD measurements that were performed with UHF antennas to fulfill the goals outlined in Section 1.5.

Chapter 3
Design and Testing of Antennas

This chapter will present the selection of the antenna type, antenna design specifications, and tests that were performed to verify antenna functionality. The antennas described in this chapter were used in all experiments performed for this thesis.

3.1 Selection of Antenna Type

As described in Chapter 2, various types of antennas have been used for PD experiments. Some authors chose antennas based on their physical robustness or bandwidth. Other authors appeared to choose antennas arbitrarily.

The most common antenna used for PD measurement in the literature is the rectangular microstrip patch antenna. It is also the only UHF sensor cited in IEEE 1434 [4]. Some other advantages of the microstrip patch antenna are described below:

- It is mechanically robust. This is important in a station environment that can introduce external forces, such as vibration, to the antenna.
- It is narrowband. This trait is useful for analyzing the PD response in relation to

measurement bandwidth.

- It is simple to fabricate.
- The focus of this thesis is PD measurement and not the antenna, so it is unnecessary to choose a more complex sensor. In addition, an optimal antenna for this application was not found in the literature. Therefore, the application of a microstrip patch antenna was appropriate for this research.

3.2 Design of the Antenna

In order to study the microstrip patch antenna response to PD across the entire UHF range (300 MHz - 3 GHz), three antennas were fabricated. Since station environments will introduce noise to PD measurements, the resonant frequency of two antennas were chosen in bands that are known to be noisy (900 and 2450 MHz). 1500 MHz was selected as an arbitrary intermediate frequency between 900 MHz and 2450 MHz.

A printed circuit board (PCB) manufacturer, PCBWay, fabricated the antennas using an FR-4 substrate with a dielectric height of 1.6 mm, a dissipation factor of 0.017, and a dielectric constant of 4.7. To specify the patch dimensions, the design process in [24] was followed. First, the patch width was computed using [24]

$$W = \frac{1}{2f_r\sqrt{\mu_0\varepsilon_0}}\sqrt{\frac{2}{\varepsilon_r+1}} \tag{3.1}$$

where f_r is the desired patch antenna resonant frequency, $\mu_0 = 4\pi\times10^{-7}$ H/m is the magnetic permeability of free space, $\varepsilon_0 = 8.854\times10^{-12}$ F/m is the dielectric permittivity of free space, and $\varepsilon_r = 4.7$ is the dielectric constant of FR-4. Due to the fact that patch dimensions are

finite, fringing effects exist at the edges. To account for this, an effective dielectric constant was computed using [24]

$$\epsilon_{reff} = \frac{\varepsilon_r + 1}{2} + \frac{\varepsilon_r - 1}{2}\left[1 + 12\frac{h}{W}\right]^{-1/2}. \tag{3.2}$$

In (3.2), h is the dielectric height and W is the patch width. Also due to fringing effects, the electrical length of the patch is larger than the physical length. This difference in length, ΔL, was calculated with [24]

$$\frac{\Delta L}{h} = 0.412\frac{(\varepsilon_{reff} + 0.3)\left(\frac{W}{h} + 0.264\right)}{(\varepsilon_{reff} - 0.258)\left(\frac{W}{h} + 0.8\right)}. \tag{3.3}$$

Finally, the actual patch length was calculated using [24]

$$L = \frac{1}{2f_r\sqrt{\varepsilon_{reff}}\sqrt{\mu_0\varepsilon_0}} - 2\Delta L. \tag{3.4}$$

Once the length and width were calculated for each antenna, a design file was sent to the PCB manufacturer for fabrication. The top PCB layer contained the rectangular patch, and the bottom layer contained the ground plane. The ground plane dimensions (and thus the entire sensor dimensions) were chosen to be $2L \times 2W$.

3.2.1 Feed Points

To simplify the antenna fabrication process, a coaxial feed was chosen over other configurations such as a microstrip line (or inset) feed [24]. Since the cable and oscilloscope attached to each patch had a resistance of 50 Ω, the feed points were chosen such that the resonant input resistance was 50 Ω to minimize reflections. If the feed points are located halfway along each patch's width, the feed point location along the length of each patch can be computed.

Table 3.1: Calculated design parameters for each patch antenna.

Antenna Center Frequency [MHz]	**Patch Width [mm]**	**Patch Length [mm]**	**Feed Point Along Length of Patch y_0 [mm]**
900	98.6	76.7	20.7
1500	59.2	45.9	12.5
2450	36.2	27.9	7.7

The first step in calculating the feed point location of each patch is finding the conductance of the patch's radiating slots (which are the areas between conductors at the edges of the patch along the width) which is given by [24]

$$G_1 = \frac{1}{90}\left(\frac{W}{\lambda_0}\right)^2. \tag{3.5}$$

In (3.5), λ_0 is the wavelength at the patch's resonant frequency. Next, the resonant input resistance at the edge of each patch was calculated, ignoring the mutual effects of slots using [24]

$$R_{in} = \frac{1}{2G_1}. \tag{3.6}$$

The feed point coordinate y_0 was then calculated with [24]

$$R_{in}(y = y_0) = R_{in}(y = 0)\cos^2\left(\frac{\pi}{L}y_0\right) \tag{3.7}$$

where $R_{in}(y = y_0)$ is the desired input resistance at the feed point (which is 50 Ω) and $R_{in}(y = 0)$ is the input resistance at the edge of the patch.

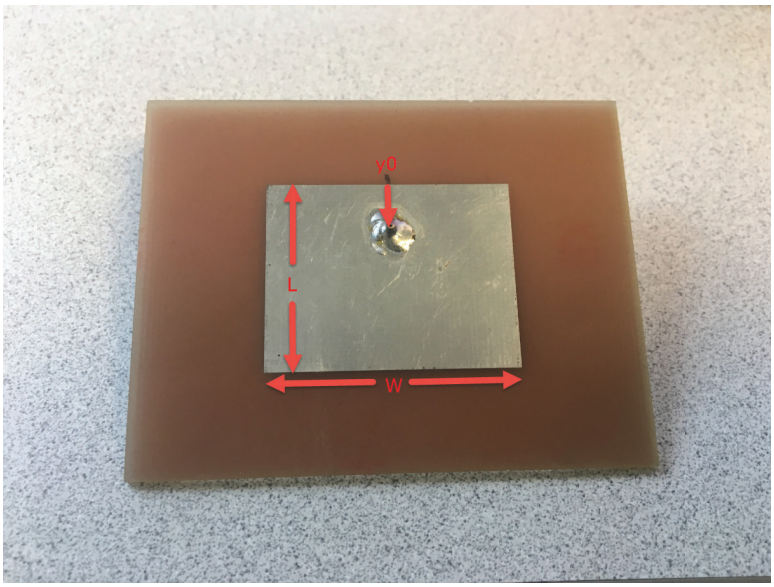

Fig. 3.1: Photo of 2450 MHz patch antenna and the location of the feed point.

Once the antennas were fabricated, the feed points were drilled at the correct locations and female SMA connectors were soldered to the patches. The calculated design parameters for each antenna are shown in Table 3.1. A photo of the 2450 MHz patch is shown in Fig. 3.1.

3.3 Verification of Antenna Design

Before using the patch antennas for PD experiments, some measurements were performed to ensure that the antennas were functioning properly. These included scattering parameter measurements and tests with a commercial UHF calibrator.

3.3.1 Scattering Parameters

To determine the resonant frequency and bandwidth, and to verify the impedance matching of each antenna, S_{11} measurements were performed with a VNA. As discussed in Section 2.3.1, S_{11} measures the reflected voltage when an incident wave is applied to a circuit port at a particular frequency. If the connected specimen is a patch antenna, the minimum value of S_{11} will occur at the dominant resonant frequency because at that frequency, a significant amount of energy applied to the antenna should radiate if the resonant input impedance (determined by the feed point) is adequately matched to the VNA port and cable.

Figure 3.2 shows the S_{11} measurements up to 2 GHz on the 900 MHz antenna. The first minimum S_{11} value occurred at 927 MHz which is the TM_{010} dominant mode. The -10 dB bandwidth at this frequency was 6.6 MHz. The VNA also measured resonances at 1457 MHz (TM_{002} mode) and 1754 MHz (TM_{020} mode). Field modes were verified with theory using the measured antenna dimensions and (14-33), (14-34), and (14-35) in [24].

The S_{11} measurement on the 1500 and 2450 MHz antennas is shown in Figs. 3.3 and 3.4, respectively. The 1500 MHz antenna had a measured resonant frequency of 1533 MHz and a -10 dB bandwidth of 25 MHz. The 2450 MHz antenna had a measured resonant frequency of 2498 MHz and a -10 dB bandwidth of 60 MHz. With increasing resonant frequency, the bandwidth increases because of increased losses (and lower quality factor). Only the TM_{010} mode resonant frequencies were measured on the 1500 MHz and 2450 MHz antennas because resonant frequencies of other modes are expected at frequencies above the measurement window of the VNA which was 3 GHz.

These measurements confirmed that all three rectangular patch antennas were fabricated successfully. Measured resonant frequencies differed slightly from the specified values, but this is expected due to fabrication and material tolerances, and also the approximate nature

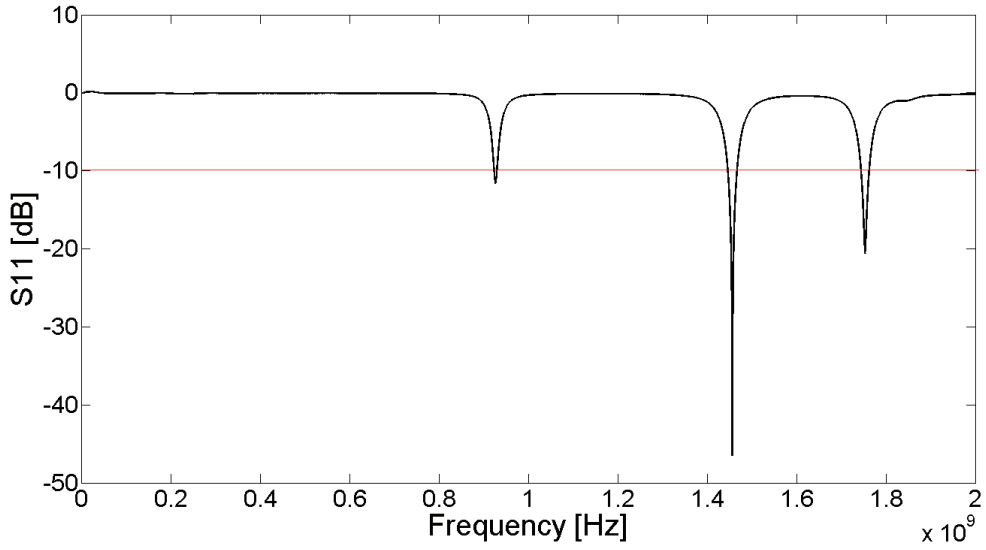

Fig. 3.2: S_{11} measurements for the 900 MHz patch antenna. Three minima appeared at 927, 1457, and 1754 MHz respectively.

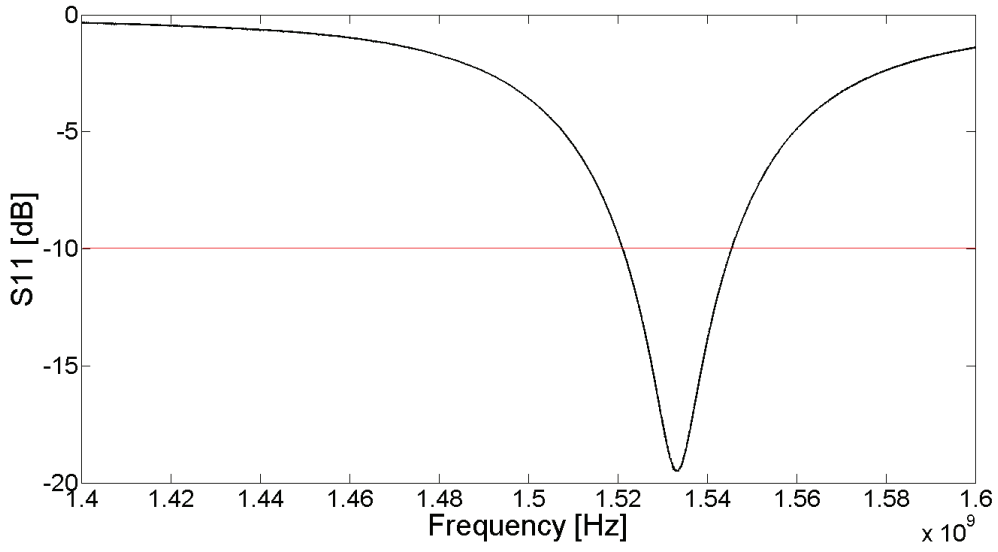

Fig. 3.3: S_{11} measurements for the 1500 MHz patch antenna. The minimum appeared at 1533 MHz.

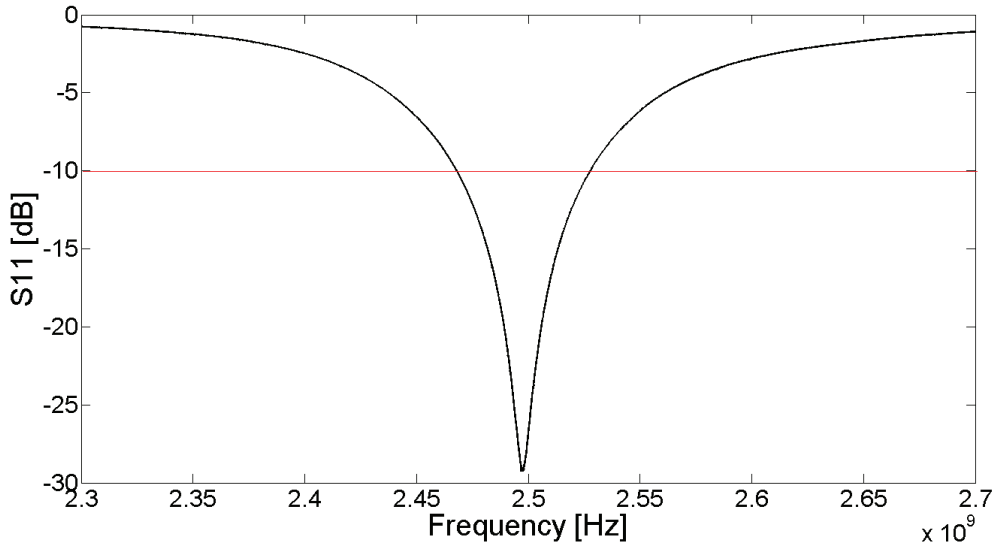

Fig. 3.4: S_{11} measurements for the 2450 MHz patch antenna. The minimum appeared at 2498 MHz.

of the design equations.

3.3.2 Measurements with a UHF Calibrator

As discussed in Section 1.3.4, it is not practical to calibrate for charge on rotating machine windings. However, a UHF calibrator can be used to inject pulses that contain frequency content similar to PD pulses in order to verify the operation of the antennas. Figure 3.5 shows the pulse from a commercial UHF calibrator[1] injected directly into a 50 Ω load. This pulse generated by the UHF calibrator was found to have a rise time of 0.5 ns and a fall time of 200 ns.

The calibrator was then used to inject voltage pulses into a stator bar placed in a grounded dummy slot (see Chapter 4 for a description of the laboratory test setup) and

[1]OMICRON UPG 620

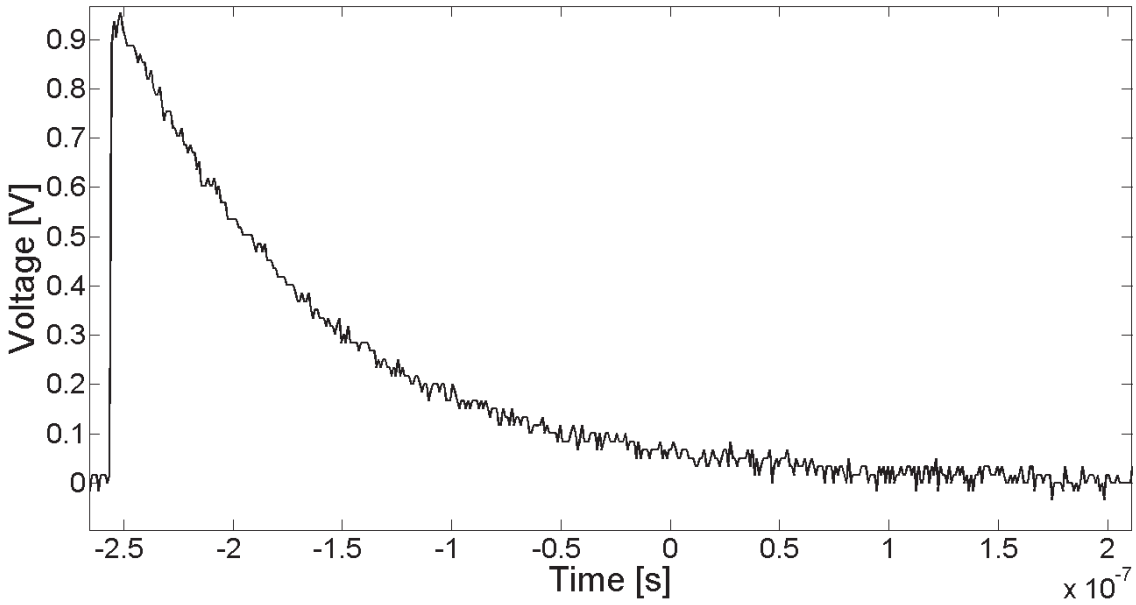

Fig. 3.5: 1 Vp UHF calibrator pulse injected into 50 Ω. The rise time was 0.5 ns and the fall time was 200 ns.

the antennas fabricated for this work were used to measure the fields radiated by the bar. The calibrator pulse signal was split between a 50 Ω cable that was connected to the stator bar and another 50 Ω cable that was connected to an oscilloscope channel (terminated in 50 Ω) to measure the injected pulse. Figure 3.6 shows the injected pulse and the 900 MHz patch antenna response. The pulse injected into the stator bar (shown in Fig. 3.6) had a rise time of approximately 1 ns, compared to 0.5 ns when the pulse was injected directly into a 50 Ω load.

Injected pulses were in the range of Volts, however the voltage of the antenna response was in the range of millivolts. High frequency pulses were reflected at the test transformer connection and the remote (open) end of the bar, creating distortions and oscillations in the response waveform and the injected pulse waveform. The antenna response waveform was

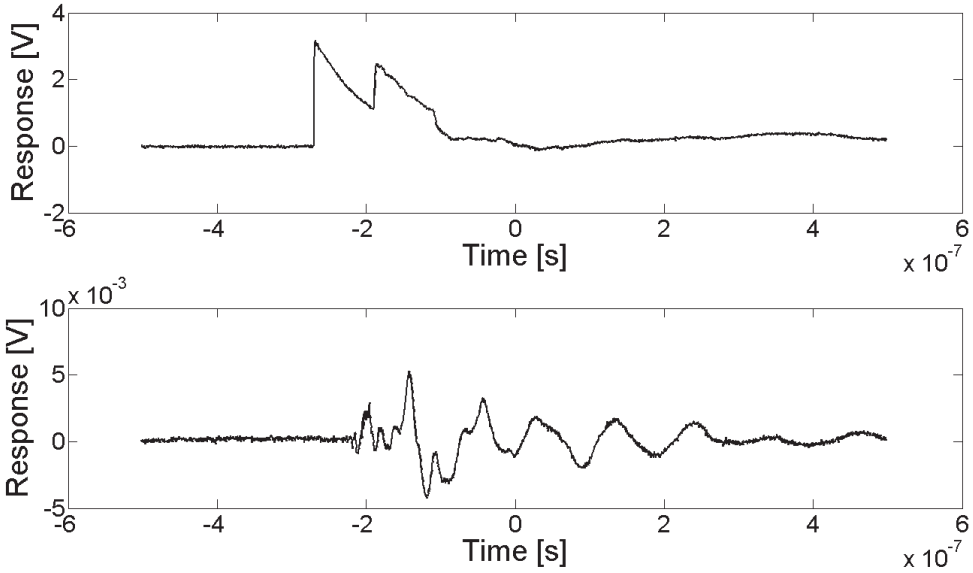

Fig. 3.6: 5 Vp UHF calibrator pulse probed with a 50 Ω measurement impedance (top) and the response from the 900 MHz patch antenna (bottom).

also different than the injected pulse waveform due to the narrowband characteristic of the antenna. For this research, it is not important to measure the exact PD pulse waveform. It is important, however, to accurately measure the pulse phase location (relative to one 60 Hz power cycle) and to calculate a magnitude that contributes to a meaningful PRPD pattern.

All three antennas responded to pulse injections up to 1.93 metres away from the test specimen, which is the maximum distance from the specimen within the laboratory's designated test area. This meant that if radiated PD had similar frequency content and strength as the calibrator signal, the antennas should be capable of providing a response.

3.4 Summary of Antenna Design Process

In this chapter, the process for designing three microstrip patch antennas (radiating at 900, 1500, and 2450 MHz) was described. It was shown that the antennas operated as designed and that the feed points were chosen appropriately. Therefore, the antennas were deemed to be ready for PD experiments.

Chapter 4

Laboratory Measurement Setup and Test Plan

This chapter presents the equipment and methodology used in the laboratory to perform high voltage PD measurements on Roebel bars using the patch antennas that were designed (in Chapter 3). This chapter also discusses the specimens chosen for experimentation and how PRPD patterns were produced with the acquired data.

4.1 Description of High Voltage Test Circuit

High voltage experiments were performed in the Materials Lab within Manitoba Hydro's High Voltage Test Facility. The designated test area was surrounded by a metallic cage which helped create an environment with relatively low background noise. A high voltage circuit was assembled in this area.

The high voltage circuit is shown in Fig. 4.1. The first variac enabled control of the output voltage. This stage also contained protection and control circuitry which is not shown in the diagram. The second variac stage was used to ensure the maximum test voltage was limited to avoid unnecessary damage to the test specimens. The output of this variac was

connected to two low voltage terminals of the high voltage test transformer.

The test transformer's maximum output was 60 kV, but the second variac limited the voltage to approximately 33 kV. The test transformer's high voltage output was connected to the test specimen. It was also connected to a 100 pF capacitive divider which enabled measurement of the output voltage with a DC voltmeter (0.1 V DC measured by the voltmeter corresponds to 1 kVrms AC at the test specimen). Additionally, the test transformer's high voltage output was connected to an 80 pF coupling capacitor and then to a commercial PD instrument used for measuring online rotating machine winding PD which had an input resistance of 50 Ω. A 500 Ω resistor was placed in shunt with the commercial instrument to limit the voltage if the commercial instrument became disconnected.

The remaining two low voltage terminals of the test transformer were connected to an analog voltmeter, which provided a redundant form of voltage measurement, and a capacitive divider which provided a low voltage AC signal that was in phase with the high voltage output. This low voltage signal was used to provide a 60 Hz phase reference for PRPD patterns (see Section 4.3.1).

4.2 Test Method

Using the laboratory setup, a high voltage was applied (8 kV to 16 kV) to individual Roebel bars to produce PD that could be detected by a commercial instrument[1] as well as UHF patch antennas. This section will provide an overview of the test methodology and specimen selection.

[1] IRIS TGA-BP

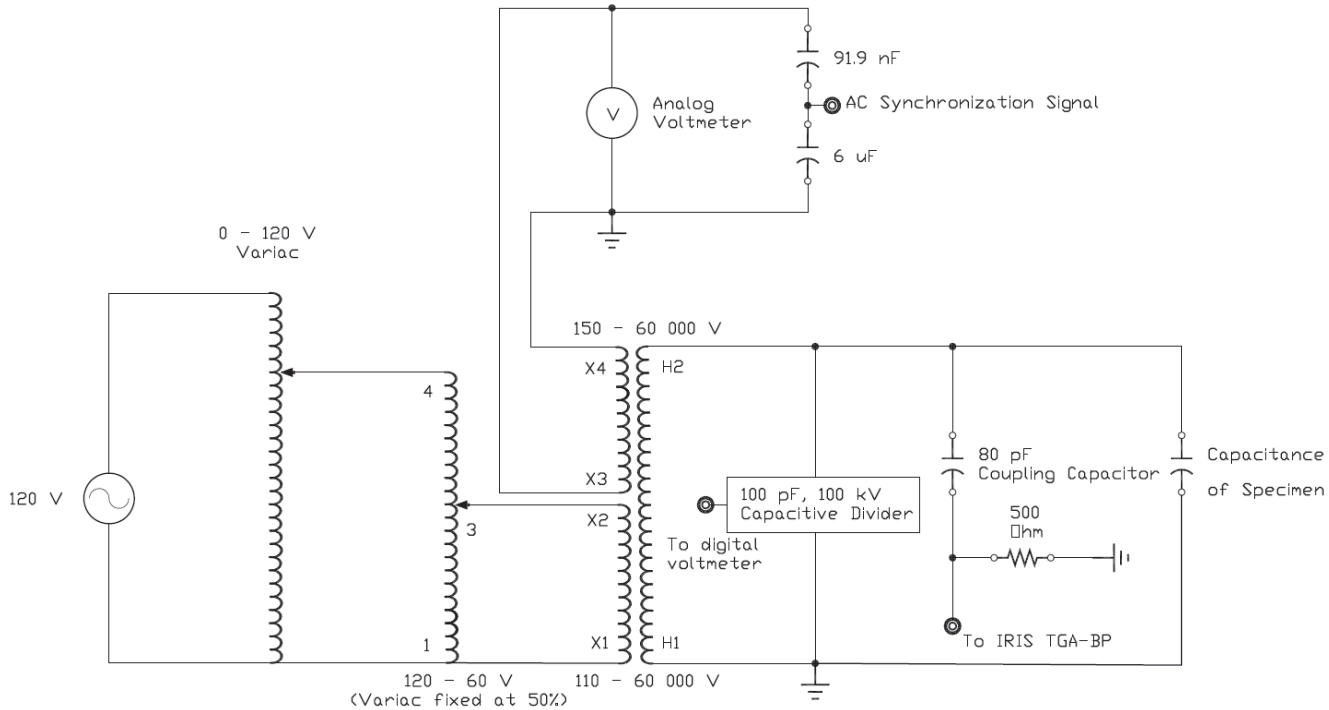

Fig. 4.1: High voltage test circuit.

4.2.1 Selection of Test Specimens

Three specimens were chosen for this work to provide enough data for useful analysis. In November 2017, a stator winding at Manitoba Hydro's Long Spruce Generating Station experienced a ground fault due to the insulation failure of one Roebel bar in the stress control region. In the aftermath of this event, a visual inspection of surrounding bars was conducted and bars suspected to have similar issues were removed from the generator (and replaced with new bars). Two of the replaced bars were chosen for this work since they were expected to produce PD in their stress control regions. The bars are designated "Long Spruce Bar 245" and "Long Spruce Bar 246" since they were removed from slots 245 and 246, respectively. It should be noted that both bars were in service since the late 1970s.

The third specimen is a Roebel bar that had short times to failure on voltage endurance according to IEEE Std. 1553 Schedule B during the manufacturing process. Inadequate flow of resin during the cure resulted in void PD, which is why this bar was chosen for experimentation. This bar was originally intended to be installed at Manitoba Hydro's Limestone Generating station, so it is designated as the "Limestone Bar" in this thesis.

Both bars are rated for 13.8 kV and have epoxy mica insulation systems. In order to simulate the electric field distribution experienced in-service, the bars under test were placed in a grounded dummy slot which mimics a stator slot (see Fig. 4.2). Since all bars were the same size, only one dummy slot was required. The specimens were initially tested without any modifications. However, if the PD response was weak, a defect was created by shorting out the stress control region(s) with semiconductive tape.

As discussed in Section 1.2.1, stator windings of many hydrogenerators are made with multi-turn coils. Multi-turn coils were not used for these experiments simply because adequate data was acquired with the Roebel bars.

Fig. 4.2: Grounded dummy slot.

4.2.2 Test Voltage and Antenna Placement

Generally, measurements were performed at 8 kV and 12 kV. 8 kV was chosen to study the level of PD in the bars that would be seen in-service. Additional voltage stress was applied to increase the PD intensity and expose defects that did not produce PD at the in-service voltage. Voltage was limited to 12 kV for Long Spruce bars since they were in-service for over three decades and it was unknown whether additional voltage stress would cause them to fail. Most measurements on the Limestone Bar were limited to 12 kV to be consistent with measurements on Long Spruce bars, but some measurements were performed at 16 kV with the stress control regions intact.

To study the effect of antenna placement relative to the specimen, three locations were chosen as depicted in Fig. 4.3. Measurements at position P1 were made with the antenna placed longitudinally away from the bar's remote end, with the patch perpendicular to the

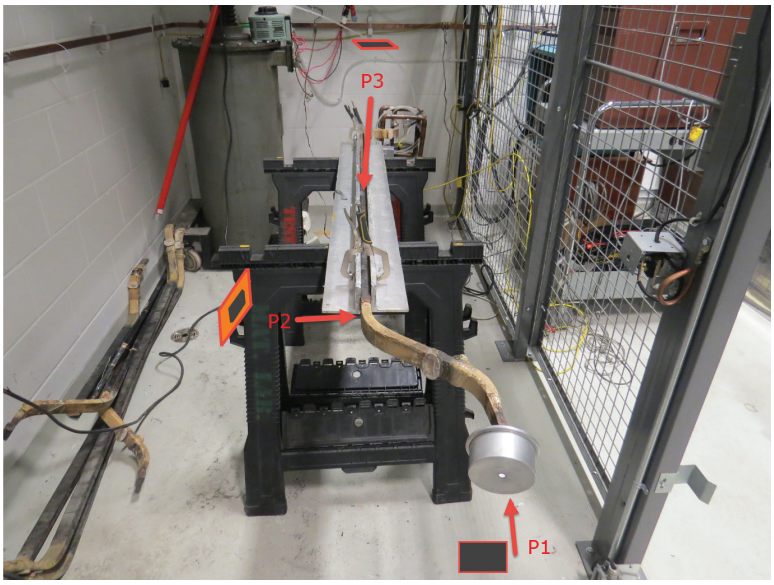

Fig. 4.3: Three selected antenna positions relative to a Roebel bar.

bar's length. Measurements at position P2 were made with the patch placed parallel to the bar's length near the stress control/slot coating interface. Measurements at position P3 were made with the patch facing the grounded slot portion of the bar (facing downward). At each measurement position, the antenna distance was altered. At P1 and P2 positions, measurements began with an antenna distance of 20 cm from the bar, and the distance was increased in increments of 20 cm until either the response from the antenna was too small to be detected or there was no more space to move further away in the test cage. Measurements in the P3 position were not sensitive (this will be discussed later), so antennas were kept close to the bar (within 10 cm) at this position. At each antenna position, antenna distance from the bar and voltage level, a measurement was attempted with all three antennas.

4.3 Data Acquisition and Processing

During each experiment, the antenna used for testing was connected to one channel of a 20 GS/s, 4-channel oscilloscope[2] (see Fig. 4.4) using a 4.6 m length of RG-58 cable. The first 4.3 m segment was connected directly to the antenna at one end, and the other end was connected to a male SMA to male BNC transition. A 30 cm BNC cable connected this transition to the oscilloscope (see Fig. 4.5). A long length of cable was required to ensure that it reached the oscilloscope at every test position. In order to create PRPD patterns, a 60 Hz AC phase synchronization signal was required (see Fig. 4.1). This signal was connected to the second channel of the oscilloscope.

Except where PD response was particularly poor, the oscilloscope was capable of storing 1000 waveforms with its segmented memory function. The waveforms were saved to a USB drive for post-processing.

4.3.1 Generation of PRPD Patterns

As discussed in Section 1.3.2, a PRPD pattern is a collection of data points representing the magnitude of individual PD pulses plotted against their phase locations in one 60 Hz cycle.

Commercial PD measurement systems contain proprietary hardware and software that calculate a magnitude from each PD waveform. For rotating machines, the peak pulse magnitude is typically used to create a PHA plot (see Section 1.3.2) which is used to calculate a quantity called Qm which is the magnitude at which the pulse repetition rate is 10 pulses per second [4]. Alternatively, the PHA plot can be used to calculate the Normalized Quantity Number (NQN) [4], which represents the normalized area under the PHA plot curve. Qm and NQN are calculated for both positive and negative PD pulses. To accomplish the objectives

[2]Keysight DSO-X-6004A

Fig. 4.4: High speed oscilloscope used for UHF PD measurements.

Fig. 4.5: RG-58 cable assembly that connects to the antenna (at male SMA end) to the oscilloscope (male BNC end).

of this thesis, it was not important to calculate these particular quantities; however, a method of calculating a PD magnitude from each waveform was required. As seen in Fig. 3.6, the high voltage circuit in the laboratory creates low frequency reflections that are coupled to the cable connecting the antenna to the oscilloscope. In most cases, the peak value of each waveform is not from the original PD response, but rather the oscillations from the circuit. Since the oscillations are generally symmetrical about 0 V, it was decided to use the Mean Differential Energy (MDE) of each waveform as the magnitude of each PD pulse. The MDE is described by the equation [42]

$$\hat{E} = \sum_i k_i (x_i)^2, k_i = \begin{cases} +1 & \text{if } x_i \geq 0 \\ -1 & \text{if } x_i < 0 \end{cases} \tag{4.1}$$

where x_i contains data points from the sampled PD signal. The MDE as described in (4.1) suppresses symmetrical noise by summing the square of all data points in the signal, x, while retaining each data point's original polarity. Therefore, the MDE should represent the initial response to the PD event which is asymmetrical in nature.

To calculate the phase location of each PD pulse, the following process was devised and implemented:

1. Prior to the acquisition of each PD dataset, acquire a few cycles of the 60 Hz synchronization signal. Since the synchronization signal is taken from a capacitive divider placed downstream from the variacs, the amplitude of this waveform will vary with test voltage. Therefore, acquiring a sample of the waveform before each PD acquisition will ensure that an accurate amplitude is recorded.

2. While acquiring PD response waveforms, simultaneously acquire the 60 Hz synchro-

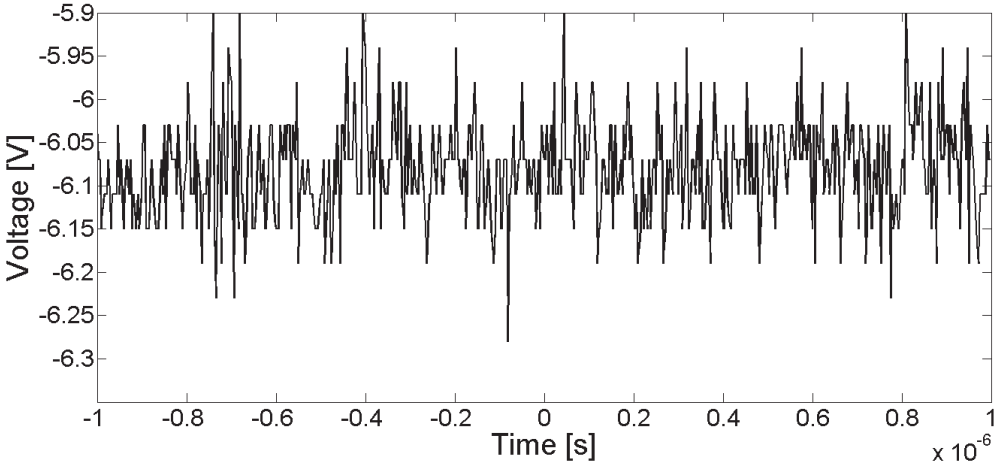

Fig. 4.6: Example of the AC reference signal acquired during a PD pulse acquisition.

nization waveform in the same time base as the PD pulse.

3. Using the 60 Hz synchronization signal amplitude and its magnitude and slope at the time of each PD pulse, the phase of each PD pulse can be calculated.

While this method was sound in theory, it was found to be unreliable after some initial experiments. Since the PD pulse capture window was extremely small compared with the time period, the magnitude of the 60 Hz signal remained almost constant and was overwhelmed by noise. Also, there was variation in the phase reference signal (see Fig. 4.6). This resulted in unreliable slope measurements which placed some PD pulses in the wrong quadrants.

Since the 60 Hz signal's slope could not be relied upon, another method of calculating the pulse phase location was devised. First, it is known that the positive peak occurs at a phase angle of $\frac{\pi}{2}$. Using the synchronization signal acquired prior to PD pulse measurement, the time corresponding to a positive peak, T_p, was determined. Then, using the radial frequency

of the 60 Hz voltage source, $\omega = 2\pi 60$ rad/s, a phase shift was calculated using

$$\phi = \frac{\pi}{2} - \omega T_p. \tag{4.2}$$

If ωT_p occurs at multiples of $\frac{\pi}{2}$, there is no phase shift. Then, the phase location of each PD pulse is the time at which each pulse occurs, T_{PD}. The phase can then be calculated using

$$\theta^{'} = \omega T_{PD} + \phi. \tag{4.3}$$

While (4.3) should be accurate, it assumes that the power frequency is exactly 60 Hz and does not account for any drift. In order to ensure the phase location was accurate, two more steps were added. First, the result from (4.3) was converted to a phase between 0 and 2π. Then, the ratio of the magnitude of the 60 Hz synchronization signal during each PD pulse, S_{PD}, to the 60 Hz synchronization amplitude, S_p, was used to calculate the final phase value with

$$\theta = \begin{cases} \sin^{-1}\left(\frac{|S_{PD}|}{|S_p|}\right), & 0 \leq \theta^{'} < \frac{\pi}{2}. \\ \pi - \sin^{-1}\left(\frac{|S_{PD}|}{|S_p|}\right), & \frac{\pi}{2} \leq \theta^{'} < \pi. \\ \pi + \sin^{-1}\left(\frac{|S_{PD}|}{|S_p|}\right), & \pi \leq \theta^{'} < \frac{3\pi}{2}. \\ 2\pi - \sin^{-1}\left(\frac{|S_{PD}|}{|S_p|}\right), & \frac{3\pi}{2} \leq \theta^{'} < 2\pi. \end{cases} \tag{4.4}$$

This method of phase calculation has been shown to be reliable. Figure 4.7 shows the PRPD pattern produced from a needle plane PD measurement with the 900 MHz patch antenna. It is well known that PD pulses produced by a needle plane jig under voltage stress above the PDIV should occur near 90 and 270 degrees. Figure 4.7 verifies that the method of phase calculation is accurate and it also demonstrates that the 900 MHz antenna

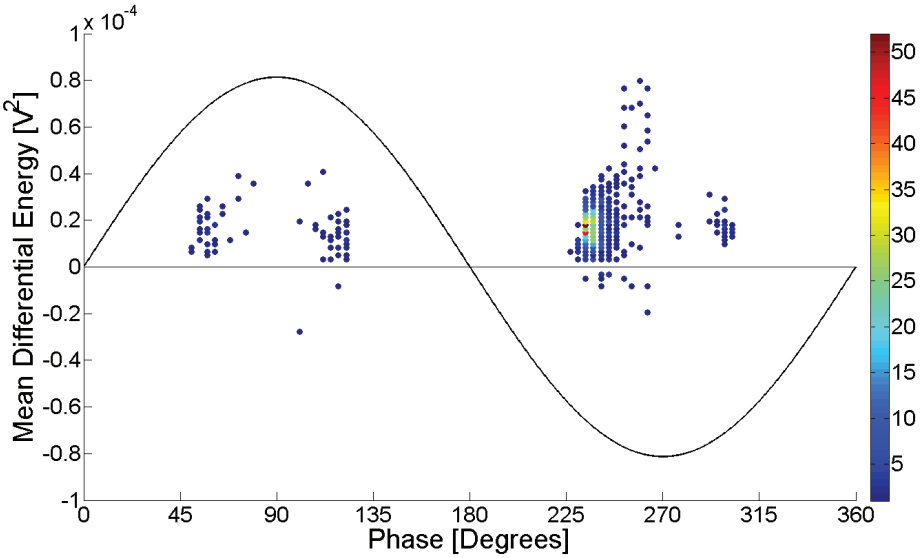

Fig. 4.7: PRPD pattern acquired with 900 MHz antenna, with 8 kV applied to a needle plane jig and the antenna placed 40 cm away.

successfully measured PD.

The colour gradient in Fig. 4.7 represents the density of PD pulses at that phase location/magnitude. The numbers on the right-hand side represent the total number of pulses recorded. To create the colour gradient, phase was subdivided into 100 windows and magnitude was subdivided into 50 windows. The number of pulses recorded in each bin was counted and used to produce the colour gradient (red indicates a high pulse density and blue indicates a low pulse density). The method of presenting PD data was used for comparing results to the data obtained with the commercial instrument which also employs a similar strategy to present data.

4.4 Conditioning Circuit

Most of the measurements in the laboratory were done with the antennas connected directly to the oscilloscope. However, some measurements were performed with an RF signal conditioning circuit in order to improve noise performance. The conditioning circuit consists of a high pass filter and amplifier placed between the antenna and the oscilloscope as shown in Fig. 4.8. The high pass filter[3] has a cut-off frequency of 800 MHz and a passband of 780-3000 MHz as specified by the datasheet. The amplifier[4] has a gain of 40 dB at 500-2500 MHz. The conditioning circuit was intended for use with all three antennas, hence the wideband characteristic of the components.

To ensure that the added components were suitable for use with the antennas, the two-port S-parameters of the signal conditioning circuit in Fig. 4.8 were measured using a VNA. To compensate for the amplifier's large gain, two 15 dB attenuators were inserted before and after the circuit. Figure 4.9 provides the measured S_{21}. The 3 dB cutoff frequency was 700 MHz. After compensating for the 30 dB attenuators, the following net gains were measured: 40.8 dB at 900 MHz, 41 dB at 1500 MHz, and 37.3 dB at 2450 MHz. These results confirmed that the conditioning circuit was suitable for use with the patch antennas and that there was a 60 dB low frequency noise rejection.

[3]Minicircuits SHP-800+
[4]Minicircuits ZX60-2534MA-S+

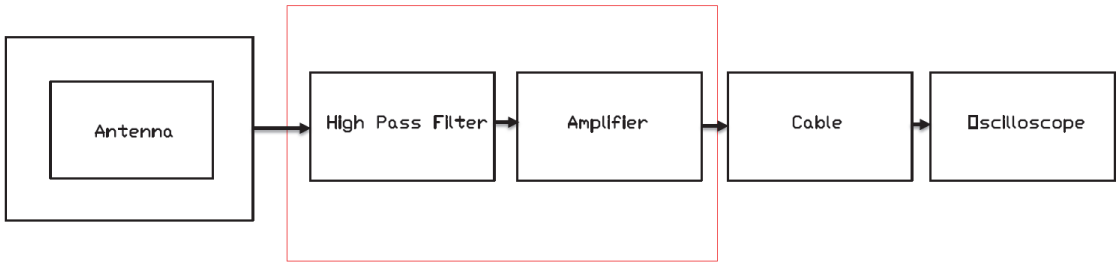

Fig. 4.8: Block diagram of the signal conditioning circuit. The components enclosed in the red box are placed near the antenna.

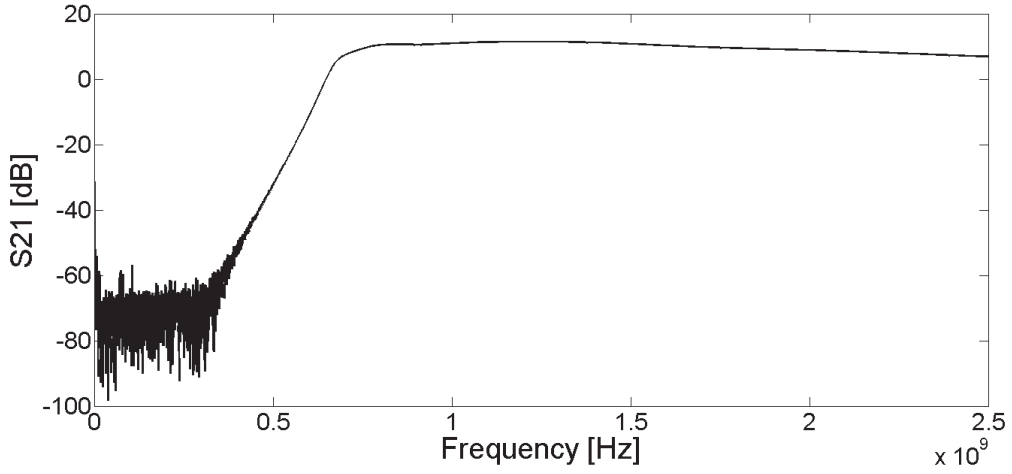

Fig. 4.9: S_{21} measurements performed on the conditioning circuit of 4.8 (the gain is reduced by 30 dB due to added attenuators).

Chapter 5
Laboratory Tests on Stator Bars

This chapter presents the results from experiments performed in the laboratory. Relevant PRPD patterns are provided using the three patch antennas in addition to PD pulse waveforms and frequency spectra. Except for the measurements in Section 5.4, all antenna measurements discussed in this chapter were performed without a conditioning circuit. Dozens of acquisitions were made with all three antennas, therefore it is not practical to show results from all measurements.

5.1 Long Spruce Bar 245

As discussed in Section 4.2.1, Long Spruce Bar 245 and 246 were selected for experimentation because they were expected to have deterioration at the stress control / semiconductive coating interface. According to IEEE 1434 and IEC 60034-27-2, the PD activity associated with this type of defect should have a positive pulse predominance with a PRPD pattern having a larger cluster at 225 degrees compared to the one at 45 degrees [4, 7].

Figure 5.1 shows the result of measurements made on Long Spruce Bar 245 with a commercial instrument using an 80 pF coupling capacitor to detect PD (see Fig. 4.1 for

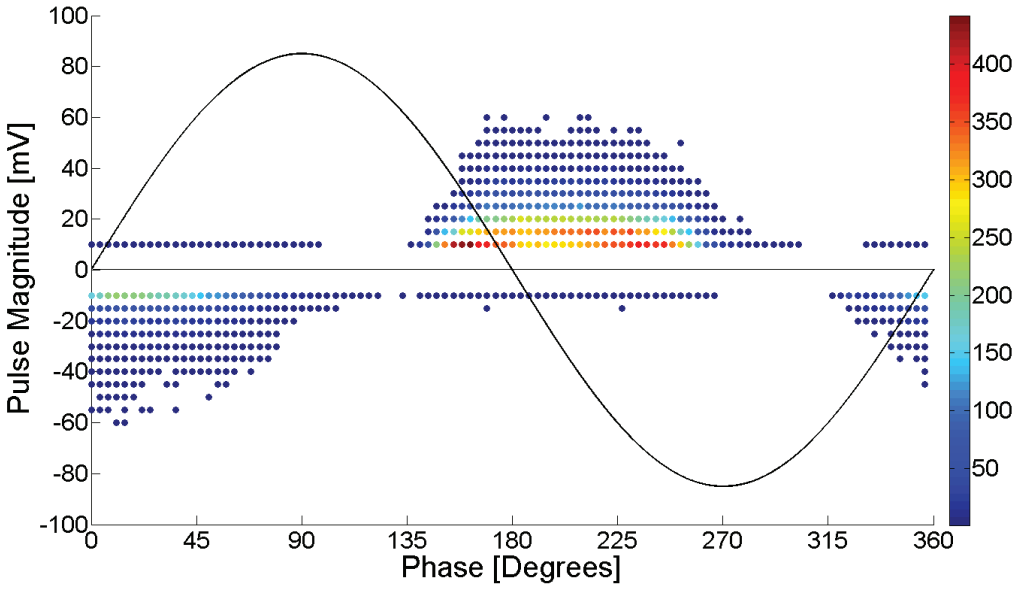

Fig. 5.1: PRPD obtained with commercial instrument while applying 12 kV to Long Spruce Bar 245.

the test circuit). The resulting PRPD pattern shows there is a positive predominance and a large cluster at 225 degrees as expected. The commercial software used to perform this acquisition calculated Qm+ = 54 mV and Qm- = 44 mV.

Initial measurements made with the three patch antennas indicated that they were not sensitive to PD generated by this specimen. It was possible to detect PD, but in some cases it took some minutes for the oscilloscope to capture 1000 pulses. From these initial tests, it was determined that the oscilloscope trigger level and settings played a significant role in the quality of the test results. Figure 5.2 is the PRPD pattern produced from an acquisition with the trigger set too low which resulted in primarily measuring background noise near 0 V.

A PRPD pattern results obtained with the 900 MHz antenna is shown in Fig. 5.3. A

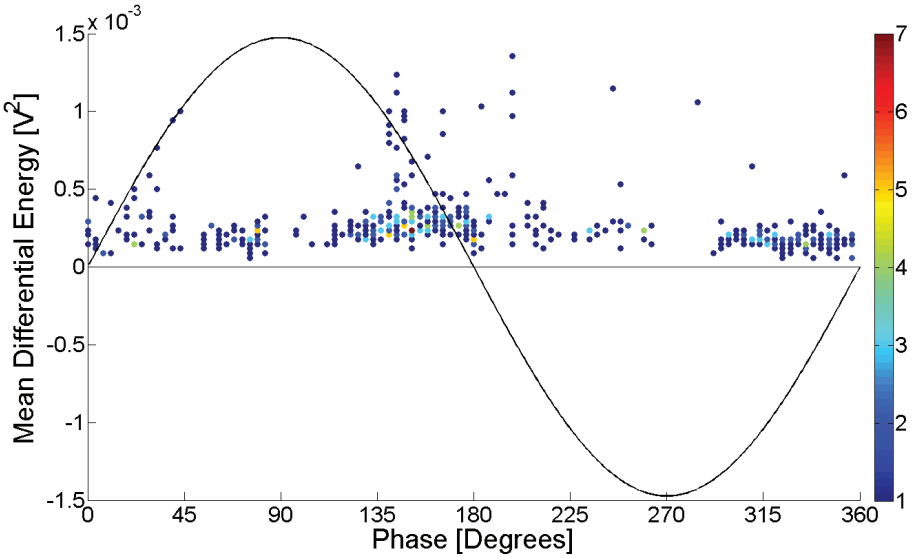

Fig. 5.2: PRPD pattern obtained with the 1500 MHz antenna in position P1 placed 20cm away from Long Spruce Bar 245 with 12 kV applied to the specimen.

positive pulse cluster in the third quadrant is apparent, in agreement with the commercial instrument, but the antenna could not detect the other activity centered around 45 degrees as depicted in Fig. 5.1.

5.2 Long Spruce Bar 246

To avoid the challenges encountered while testing Long Spruce Bar 245, semiconductive tape was used to short the stress control region at one end of Long Spruce Bar 246. With the stress control region inactive, surface PD activity near the slot exit should occur and similar PRPD patterns as Long Spruce Bar 245 should be observed. When 12 kV was applied to the bar, audible discharges could be heard near the shorted stress control region. Patch antenna measurements were performed with the antennas located near the position P2 (see Fig. 4.3).

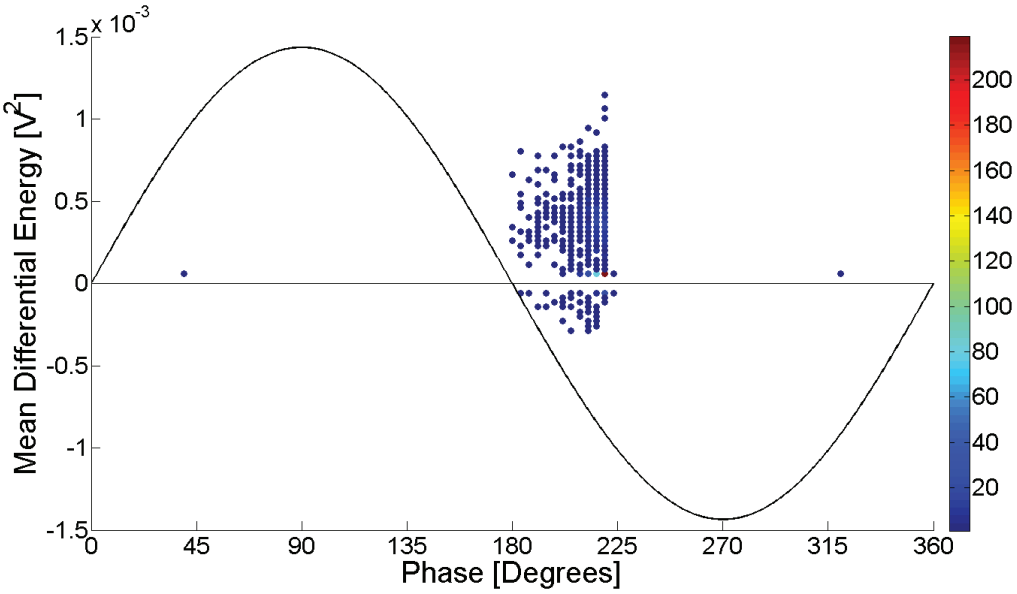

Fig. 5.3: PRPD pattern obtained with the 900 MHz antenna placed in the P1 position, 20cm away from Long Spruce Bar 245 with 8 kV applied voltage.

A PRPD pattern obtained with the 2450 MHz antenna is shown in Fig. 5.4, indicating activity at 45 degrees with a negative predominance. The oscilloscope appeared to trigger exclusively in the positive half cycle of the 60 Hz period. Upon visual inspection, one end of the semiconductive tape used to short the stress control region had delaminated and was protruding from the bar. The "sharp" conductive material created another source of PD that likely produced a large radiated field. The PRPD pattern in Fig. 5.4 has resemblance to endwinding tracking discharge as shown in the standards [4,7]. This is marked by negative predominance at 45 degrees.

The semiconductive tape protrusion was fixed and audible noise decreased. The PRPD pattern acquired with the commercial instrument is shown in Fig. 5.5. It is interesting that the PD magnitude is lower than the PD magnitude measured on Long Spruce Bar 245

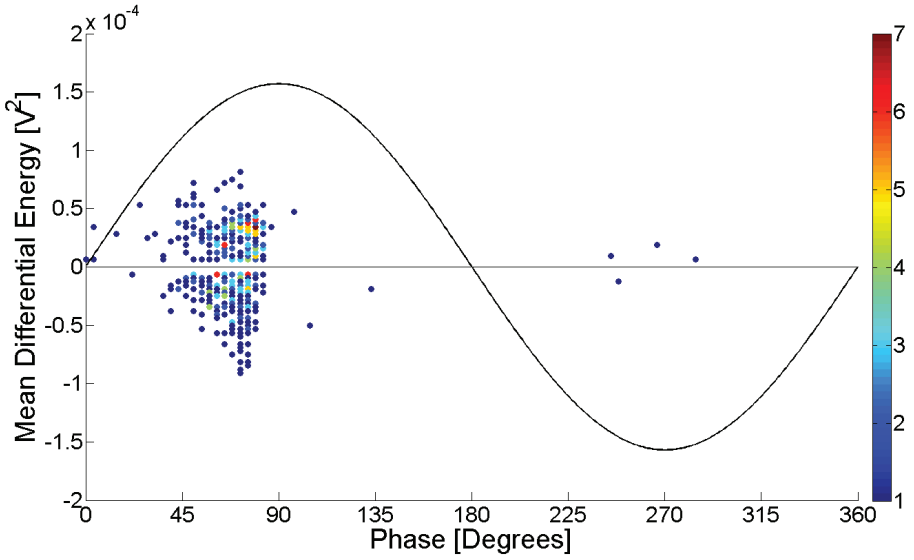

Fig. 5.4: PRPD pattern obtained with the 2450 MHz antenna placed in position P2, 20cm away from Long Spruce Bar 246 with 12 kV applied voltage. The bar's stress control region was wrapped with semiconductive tape and a part of it was protruding for this measurement.

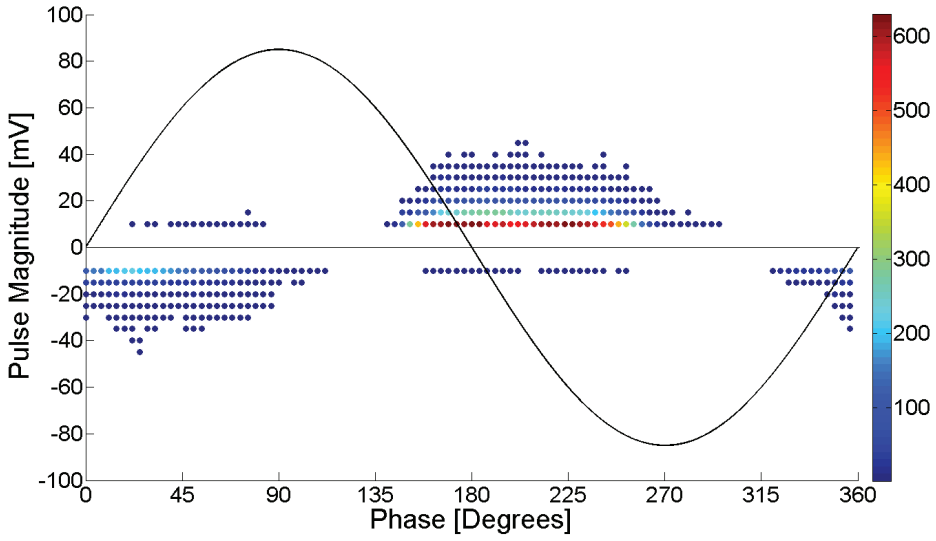

Fig. 5.5: PRPD pattern obtained with the commercial instrument while applying 12 kV to Long Spruce Bar 246 with the stress control region shorted at one end.

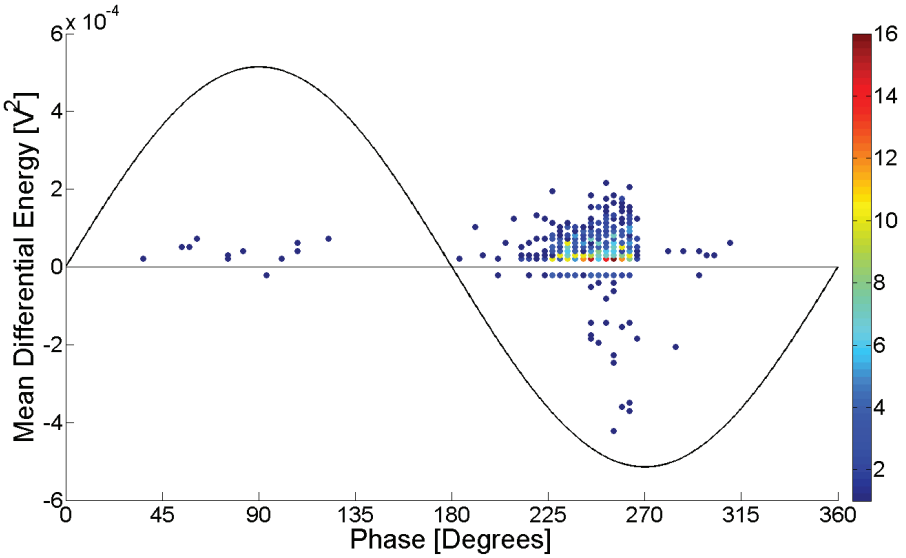

Fig. 5.6: PRPD pattern obtained with the 900 MHz antenna placed in position P1, 20 cm away from Long Spruce Bar 246 with 12 kV applied voltage.

which had its stress control regions intact. Antenna measurements were performed at all three positions (P1, P2, and P3). Measurements at positions P1 and P2 were in agreement with the commercial instrument and they were also repeatable. Figure 5.6 shows the PRPD pattern from an acquisition with the 900 MHz antenna at position P1, and Fig. 5.7 shows the PRPD pattern from an acquisition with the same antenna placed in position P2 at the same distance from the bar. While the acquisition in position P2 appeared to be more sensitive to PD (since this position is closer to the PD source), both PRPD patterns have positive pulse predominance and clusters in the third quadrant.

Measurements were made up to 60 cm away from the bar with the 1500 MHz antenna at the P2 position. PRPD patterns acquired with the antenna placed 40 cm and 60 cm from the bar are shown in Figs. 5.8 and 5.9, respectively. Both PRPD patterns indicate discharge at the stress control / semiconductive coating interface. The maximum PD magnitudes at

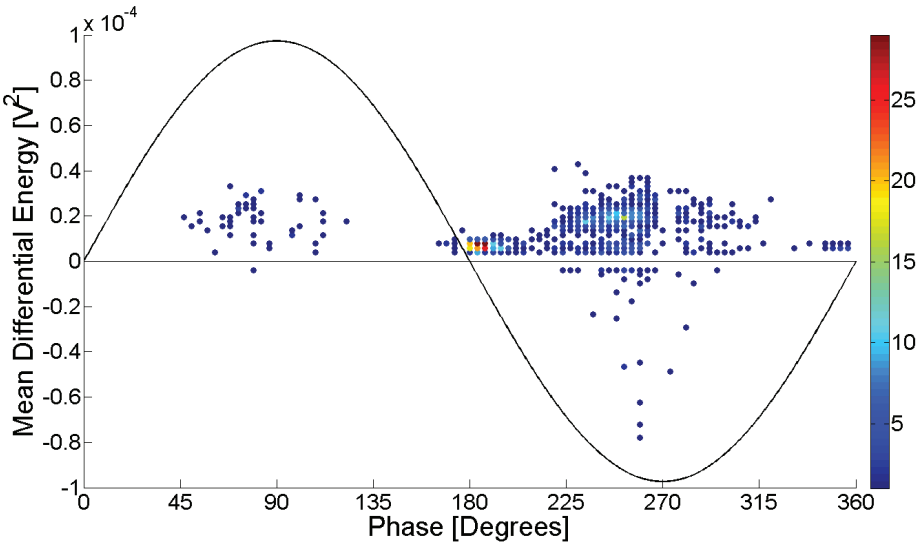

Fig. 5.7: PRPD pattern obtained with the 900 MHz antenna placed in position P2, 20 cm away from Long Spruce Bar 246 with 12 kV applied voltage.

60 cm are approximately 5 times lower than the PD magnitudes at 40 cm (according to Figs. 5.8 and 5.9). This is an expected result since the fields in the radiated far field should decrease with the distance [24]. The 1500 MHz antenna is in the radiated far field region at 40 cm (see (2.4)).

Measurements were performed with the 2450 MHz antenna, but it was much less sensitive to PD than the other antennas. The PRPD pattern shown in Fig. 5.10 indicates far fewer detected PD events than the other PRPD patterns for the 900 MHz and 1500 MHz antennas. Fifty pulses were acquired because intervals between pulses could be as long as 1 min. With the other antennas, 1000 pulses were typically acquired within 5-10 seconds.

Acquisitions were attempted in the P3 position with all antennas. This was done by fastening the antenna to one end of a hot stick and suspending the antenna above the slot section from a safe distance. In most cases, these measurements at P3 did not provide

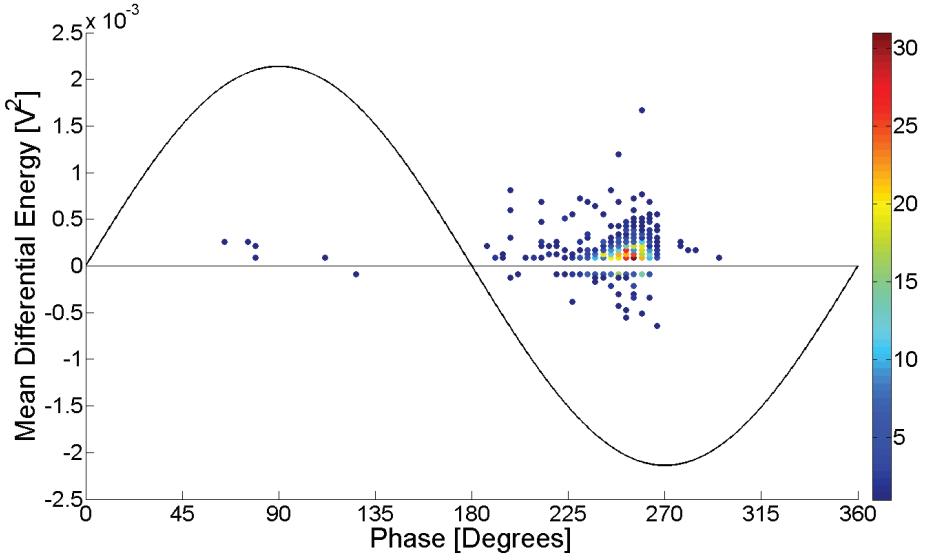

Fig. 5.8: PRPD pattern obtained with the 1500 MHz antenna placed in position P2, 40 cm away from Long Spruce Bar 246 with 12 kV applied voltage.

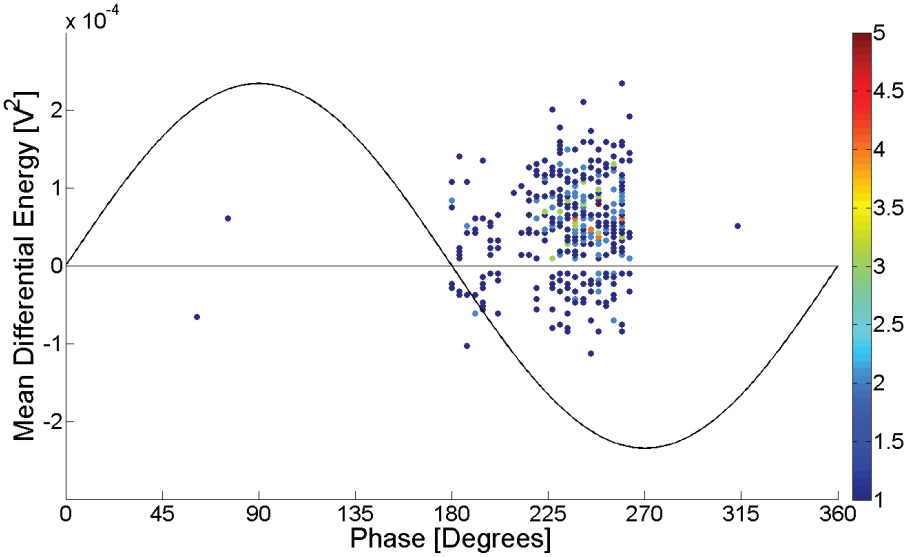

Fig. 5.9: PRPD pattern obtained with the 1500 MHz antenna placed in position P2, 60 cm away from Long Spruce Bar 246 with 12 kV applied voltage.

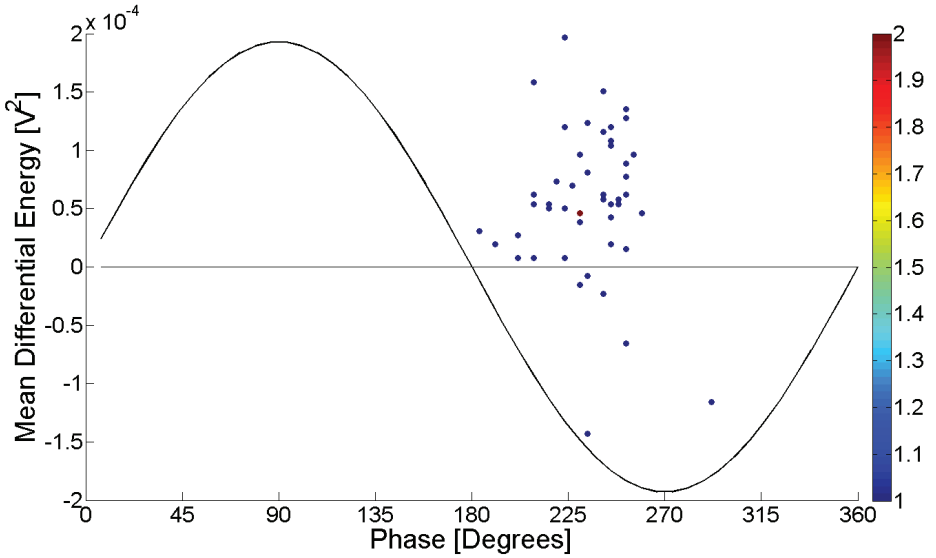

Fig. 5.10: PRPD pattern obtained with the 2450 MHz antenna placed in position P1, 40 cm away from Long Spruce Bar 246 with 12 kV applied voltage.

valid data. PD pulses were not detected beyond a distance of approximately 10 mm from the bar. When signals were detected at this position, they generally did not agree with results from other positions. One exception was observed when the semiconductive tape was protruding from the stress control region. An acquisition with the 2450 MHz antenna showed PD activity was measured in the expected phase location of 45 degrees (see Fig. 5.11). Since the semiconductive tape around the entire slot region of the bar is conductive, it is expected that PD activity is lower in this region unless there are slot discharges or other surface discharges.

Fast Fourier Transforms were performed on PD pulse waveforms acquired with each antenna to verify that radiated PD pulses contained frequency content at the antennas' center frequencies. Figures 5.12, 5.13, and 5.14 depict waveforms and spectra for the 900, 1500, and 2450 MHz antennas, respectively. By looking at the spectra, it is clear that fields

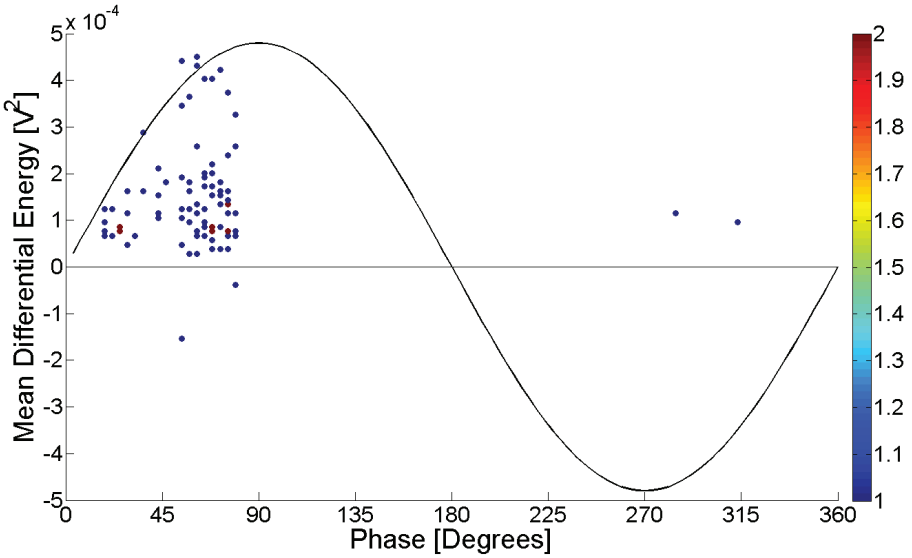

Fig. 5.11: PRPD pattern obtained with the 2450 MHz antenna placed in position P3, less than 10 mm away from Long Spruce Bar 246 with 12 kV applied voltage.

radiated from PD pulses generated from Long Spruce Bar 246 have frequency content within each antenna's bandwidth.

The results from tests on Long Spruce Bar 246 confirm that PD was radiated in the UHF range up to 2450 MHz and it was possible to measure this activity with antennas in the radiated far field.

5.3 Limestone Bar

In Section 4.2.1, it was noted that the Limestone Bar was expected to produce significant void PD activity due to issues encountered in the resin curing process during production. The PRPD pattern obtained with the commercial instrument at 16 kV applied voltage is shown in Fig. 5.15. Note that there was a strong positive pulse predominance (Qm+ = 127

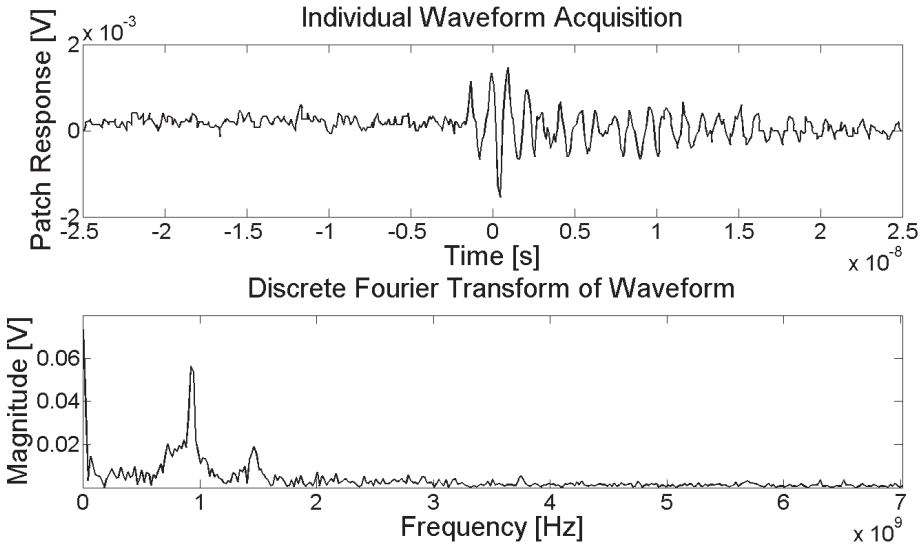

Fig. 5.12: Waveform and spectrum of a PD pulse acquired with the 900 MHz antenna in position P1, 40 cm away from Long Spruce 246 with 12 kV applied voltage.

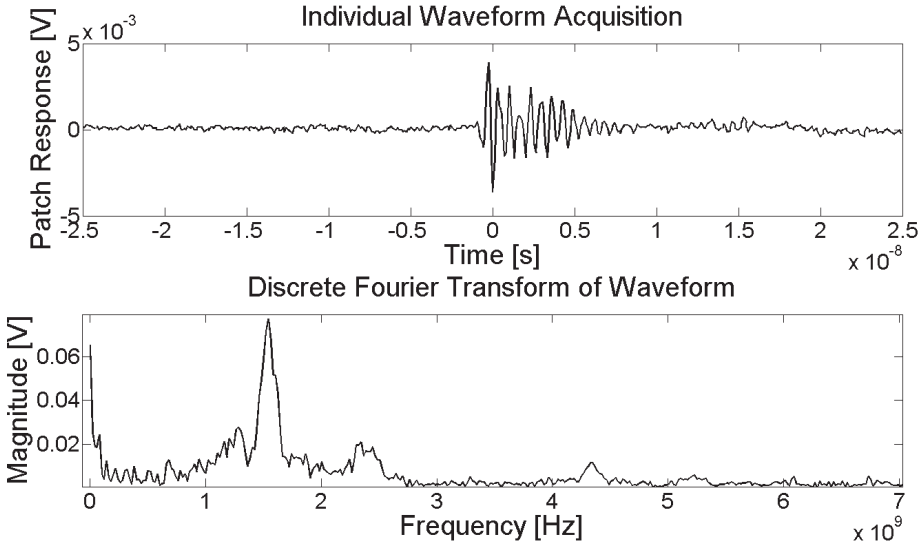

Fig. 5.13: Waveform and spectrum of a PD pulse acquired with the 1500 MHz antenna in position P2, 40 cm away from Long Spruce 246 with 12 kV applied voltage.

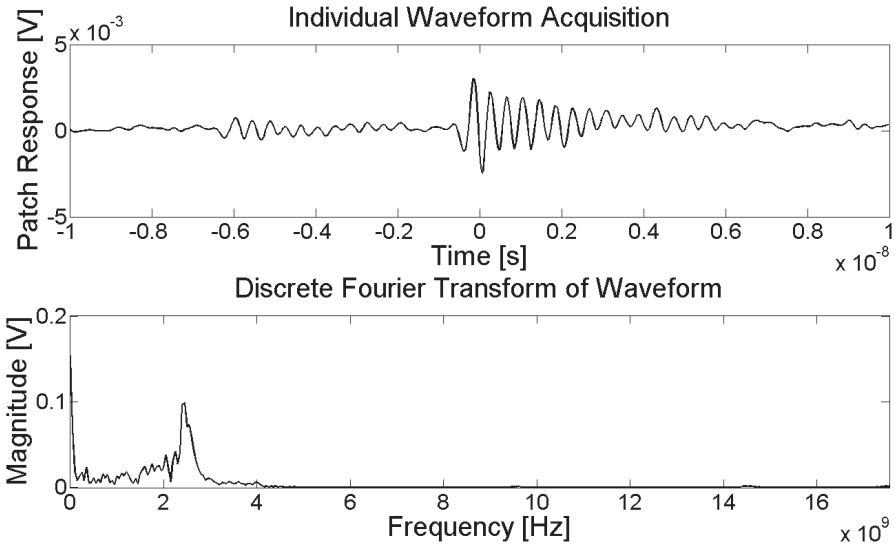

Fig. 5.14: Waveform and spectrum of a PD pulse acquired with the 2450 MHz antenna in position P2, 40 cm away from Long Spruce 246 with 12 kV applied voltage.

mV, Qm- = 42 mV).

The PRPD pattern obtained from the commercial instrument clearly indicated that the Limestone Bar had significantly higher PD magnitudes than both Long Spruce bars. As a consequence of this, the antennas were expected to be more sensitive to PD on the Limestone Bar. All antennas were able to measure PD activity, however, it was found that an appropriate trigger level setting was critical to obtain results that were similar to those obtained with the commercial instrument. Figure 5.16 is an example of an acquisition with the trigger level set appropriately to capture the large positive pulses that appear in the third quadrant of the 60 Hz period.

To demonstrate the drastic effect of the oscilloscope trigger setting, Fig. 5.17 shows a PRPD pattern obtained with the 1500 MHz antenna and a trigger setting that was set too low. Clearly, the PRPD pattern does not resemble the commercial instrument data. To

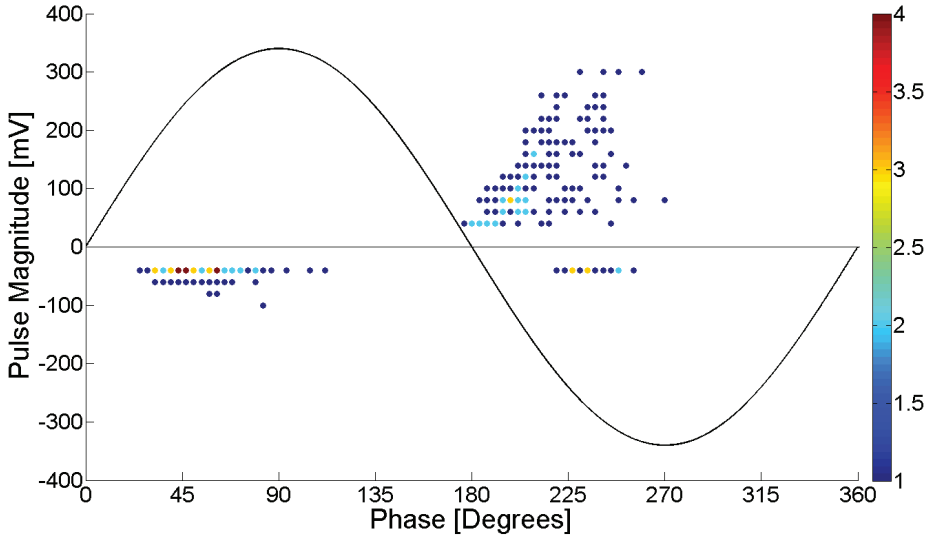

Fig. 5.15: PRPD pattern obtained with the commercial instrument using an 80 pF coupling capacitor connected to the Limestone Bar with an applied voltage of 16 kV.

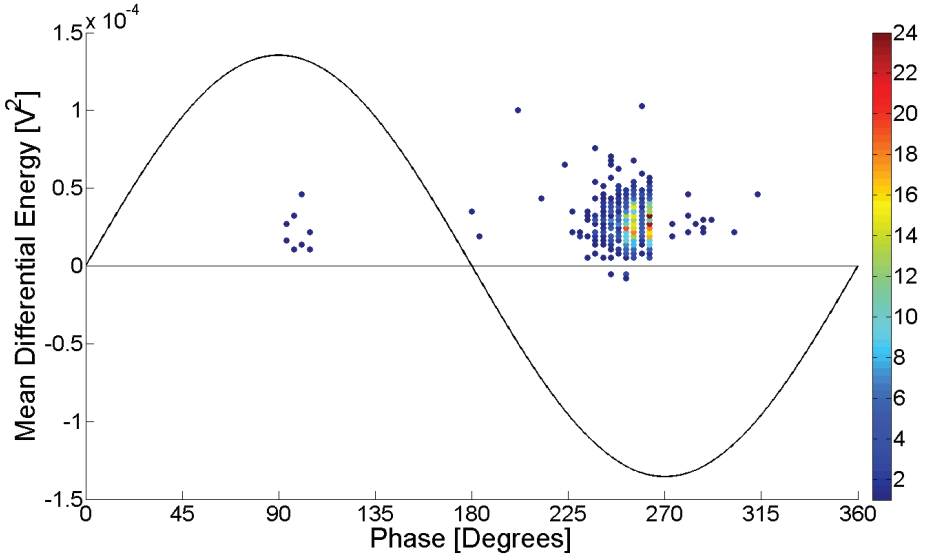

Fig. 5.16: PRPD pattern obtained with the 1500 MHz antenna placed 20 cm away from the Limestone Bar in the P1 position with an applied voltage of 16 kV.

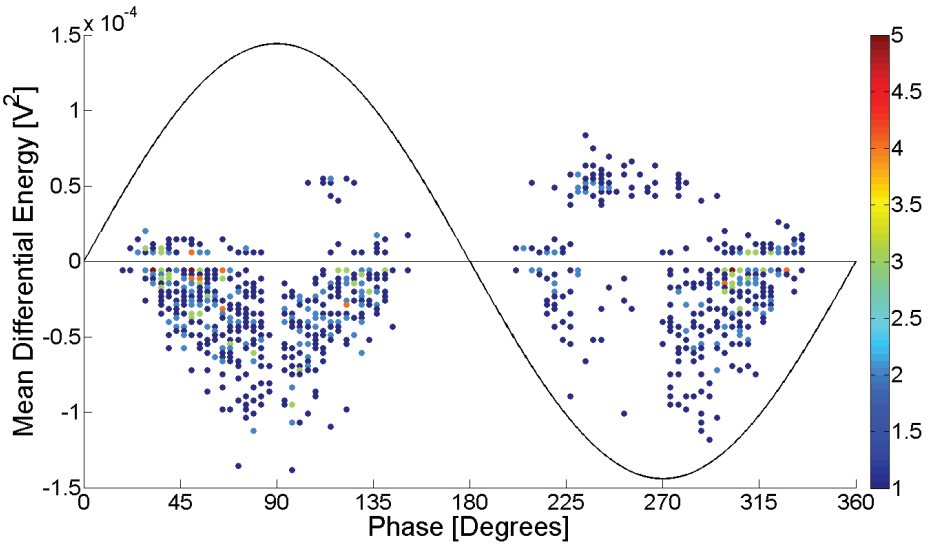

Fig. 5.17: PRPD pattern obtained with the 1500 MHz antenna placed 20 cm away from the Limestone Bar at the P2 position with an applied voltage of 16 kV and a bad trigger setting used on the oscilloscope.

demonstrate that this is due to the oscilloscope settings and not the antenna, a measurement was taken with a commercial D-Dot sensor, as shown in Fig. 5.18, which resulted in a similar PRPD pattern.

Experience with this specimen made it clear that a better method of pulse acquisition should be developed to improve the reliability of the test results.

5.4 Measurements with Conditioning Circuit

The conditioning circuit, discussed in Section 4.4, was utilized for some measurements presented in this section. Experiments were repeated on Long Spruce Bar 246 (with stress control shorted at one end) with the conditioning circuit to see if it was able to reduce noise and improve results.

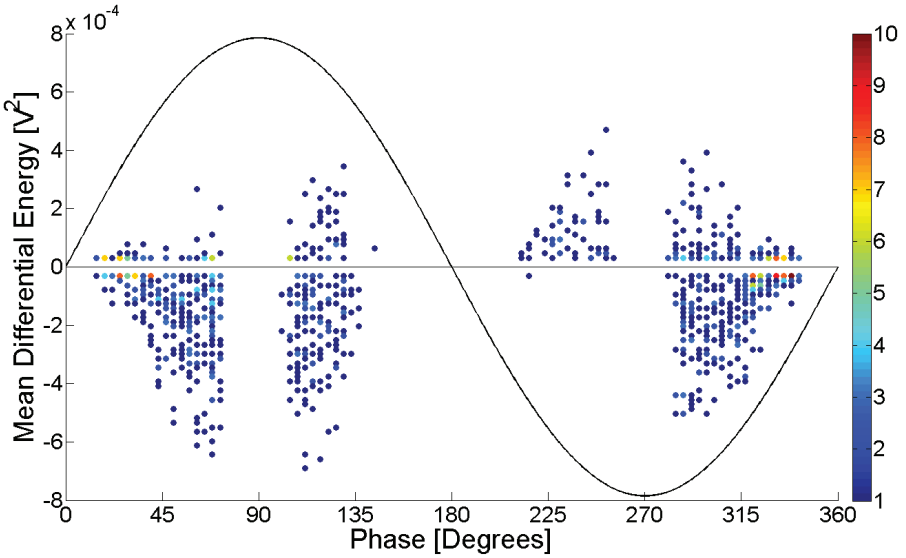

Fig. 5.18: PRPD pattern obtained with a commercial D-Dot sensor placed 40 cm away from the Limestone Bar at the P1 position with an applied voltage of 16 kV and a low trigger setting used on the oscilloscope.

As the conditioning circuit significantly increased the measured PD magnitude (similar to the Limestone bar experiments), the trigger settings had a significant impact on the results and needed to be set appropriately. The PRPD pattern obtained with the 1500 MHz antenna, shown in Fig. 5.19, indicates that a pulse predominance in the third quadrant of the 60 Hz period was measured, consistent with previous results (see Fig. 5.8 for example). In addition, PD activity was measured in the positive 60 Hz half cycle which was not previously measured. However, the conditioning circuit appeared to have a detrimental effect on pulse polarity detection.

Figure 5.20 shows an example waveform and spectrum obtained with the 900 MHz antenna and conditioning circuit. Comparing to Fig. 5.12, it is clear that the filter in the conditioning circuit functioned properly and suppressed low frequency noise.

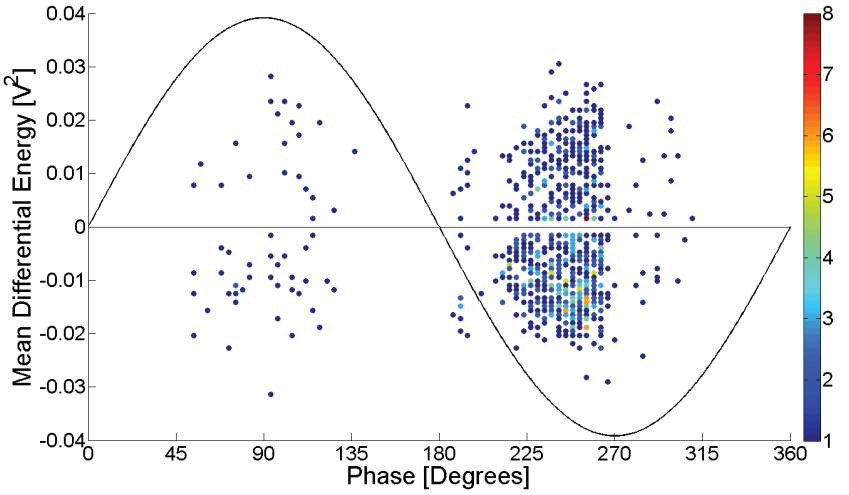

Fig. 5.19: PRPD pattern obtained with the 1500 MHz antenna placed 20 cm away from Long Spruce Bar 246 (with the stress control shorted at one end) at the P1 position with an applied voltage of 12 kV. The conditioning circuit was used with the antenna.

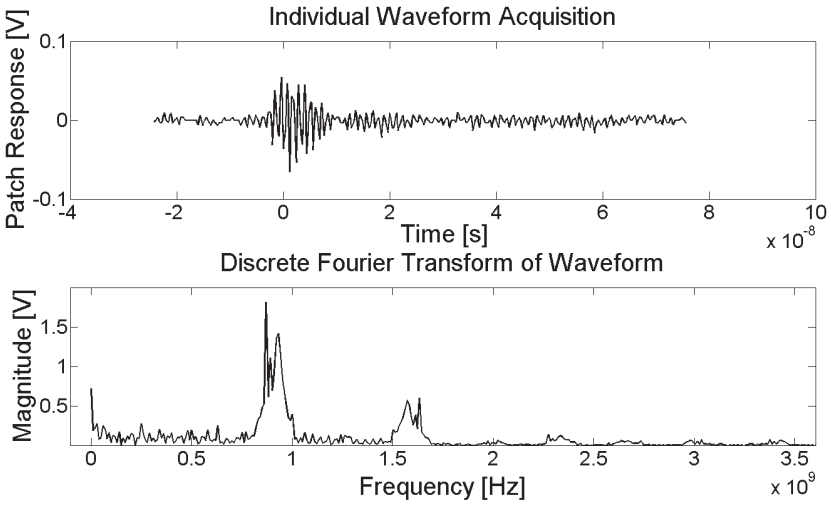

Fig. 5.20: Waveform and spectrum of an acquisition made with the 900 MHz antenna placed 20 cm away from Long Spruce Bar 246 with the stress control shorted at one end and the conditioning circuit used for signal acquisition. The applied voltage was 12 kV.

5.5 Conclusion from Laboratory Experiments

Results in this chapter confirm that UHF antennas can be used to measure PD on stator bars, despite the problems that were encountered during laboratory experiments. The results also demonstrate that the method of PD pulse acquisition and PRPD pattern production developed in this work is capable of yielding results that are comparable with those from a widely used commercial instrument.

Chapter 6
Field Tests on a Hydrogenerator

Even though successful measurements were made with patch antennas in the laboratory as described in Chapter 5, those measurements were performed in a controlled, low-noise environment which did not simulate the conditions in a station environment. Therefore, it was necessary to perform online measurements on an operating machine in order to evaluate the feasibility of the measurement technique developed in this thesis. This chapter will discuss tests performed on a hydrogenerator with UHF patch antennas.

6.1 Generator Selection and Details

Manitoba Hydro owns hydro-electric generating stations along the Winnipeg River. A review was initially conducted of recent online PD data acquired on all Winnipeg River generators with the commercial instrument[1] as part of the utility's regular test program. To optimize the chances of PD detection with the UHF patch antennas, it was preferable to select a generator with relatively high PD magnitudes. While other generators were suitable candidates, Unit 1 at Great Falls Generating Station was chosen because it had high Qm values compared to

[1] IRIS TGA-BP

other generators on the river.

Great Falls Generating Station is located approximately 25 km north of Lac du Bonnet, Manitoba. Unit 1 was originally installed in 1923 and it was rewound in 1965. Its winding has a polyester mica insulation system, and it is rated for 11 kV and 21 MVA. The winding is comprised of coils with four series turns. There are four parallel circuits per phase (a total of twelve circuits) and 36 coils per circuit. The coil pitch is seven slots.

6.2 Measurement Method

The test method for UHF antenna acquisition in the generating station was similar to that used in the laboratory. Main challenges for generating station measurements are determining appropriate antenna locations and finding a suitable 60 Hz phase reference signal for each measurement.

6.2.1 Comparisons with Commercial Instrument

To help analyze the data acquired with patch antennas, measurements with the commercial instrument were performed in order to compare PRPD patterns. As implied above, Great Falls Unit 1 is already equipped for online electrical PD measurements. Six 80 pF coupling capacitors (with ground isolation circuits) were installed at the line end of the winding. All three phases were equipped with a pair of coupling capacitors and each coupling capacitor detects PD on two parallel circuits. A triax cable connects each coupler to a panel as shown in Fig. 6.1. The physical length of the cables of each coupler pair were cut so that the electrical length from the phase terminal to the panel was the same for both couplers in a pair. This allowed the commercial instrument to perform differential measurements (as

Fig. 6.1: Panel used for online PD measurements on Great Falls Unit 1. The triax cables from coupling capacitors enter at the top of the panel.

shown in Table 1 Case 1 in [4]). Differential online PD measurements were performed with the commercial instrument for comparison with acquisitions taken with the UHF antennas.

6.2.2 60 Hz Phase Reference

Even though each coupler, ground isolation circuit, cable, and measurement impedance act together as a high pass filter to block most of the 60 Hz signal, the ground isolation circuit passes a small 60 Hz signal through a 1 kΩ resistor that appears at the coupler's output [4]. The 60 Hz signal from the coupler corresponding to the phase under test (with the UHF antennas) was used as the phase reference signal for PRPD pattern production. Figure 6.2 shows the 60 Hz waveform measured from one coupler output when terminated in 1 MΩ. In Fig. 6.2, six large pulses can be seen on each 60 Hz cycle. A portion of one cycle with two

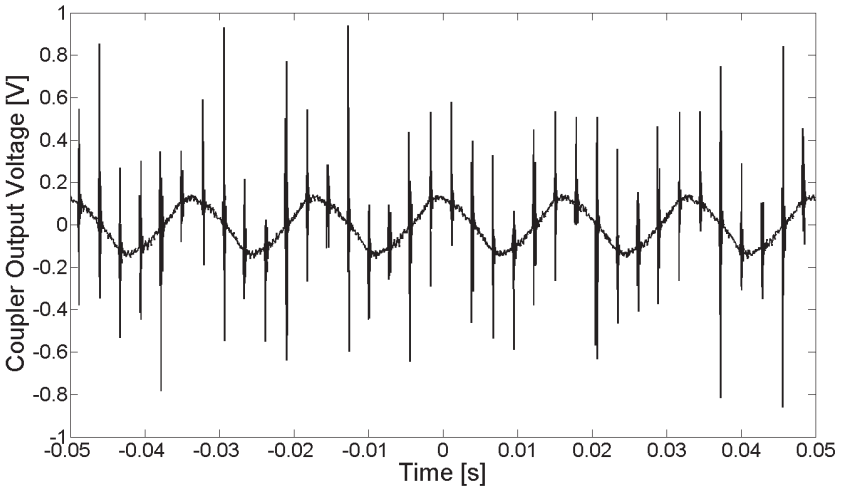

Fig. 6.2: Coupler output terminated in 1 MΩ.

pulses is shown in Fig. 6.3, along with the frequency spectrum of that signal.

The pulses originated from the static excitation system. To provide DC excitation to the rotor's field winding, a static excitation transformer is connected to the generator's 11 kV bus. The transformer steps 11 kV down to 604 V. Its low voltage winding is connected to the static excitation system which rectifies the AC voltage to DC using a six-pulse converter. Switching pulses from the converter are able to propagate to the high voltage bus and back into the generator winding where it can be detected by the PD couplers. Since the method used to produce PRPD patterns in this thesis relies on the phase reference waveform amplitude (see Section 4.3.1), digital filtering was applied to eliminate the parasitic switching pulses. It should be noted that the digital filter and panel circuitry created a 30 degree phase shift in the 60 Hz reference signal (compared to each phase's line to ground voltage) which had to be considered in post-processing.

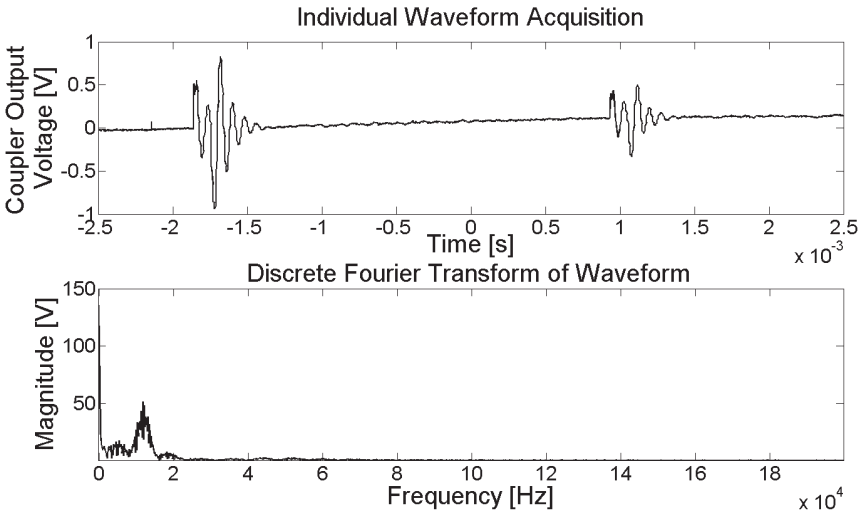

Fig. 6.3: Coupler output terminated in 1 MΩ, showing a closer view of two high frequency pulses observed in Fig. 6.2 along with their frequency content.

6.2.3 Antenna Placement

Generators at Great Falls are air-cooled and windows in the stator frame (distributed around its circumference) enable air flow (see Fig. 6.4). Conveniently, there is a line of sight to the winding overhang region through the windows near the top of the stator. The UHF antennas were placed in these windows, resembling the laboratory antenna position P2 (see Section 4.2.2). Figure 6.5 shows the antenna (and conditioning circuit) placed just inside the stator frame.

When performing high voltage tests in the laboratory on bars or coils, the conductor of the entire specimen under test is at the applied test voltage. In a stator winding that is in service, there is a linear voltage gradient from the line end (generator output) to the neutral end which is typically grounded through an impedance. In the case of Great Falls Unit 1, the line end coil should be at 6.35 kV (line to ground), the 18th coil from the line

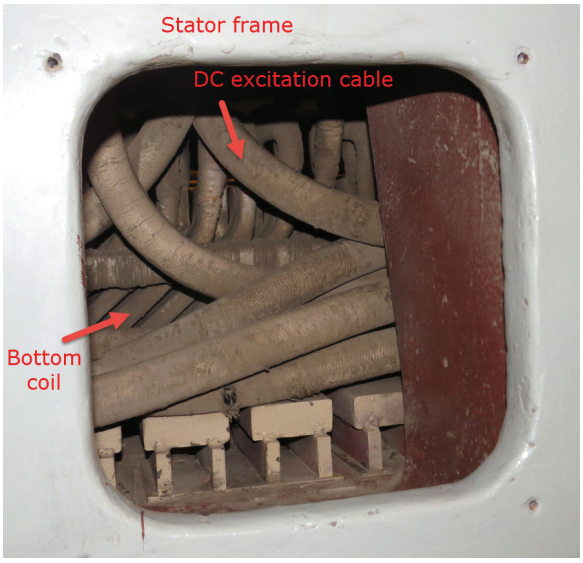

Fig. 6.4: Window in the upper region of the stator frame. The stator winding can be seen behind cables that connect the static exciter to the rotor field winding.

Fig. 6.5: Antenna placed in an upper stator frame window. The conditioning circuit is connected to the antenna and the oscilloscope is on the table next to the stator frame.

end should be at 3.17 kV and the neutral end coil should be near 0 V. Since the likelihood of PD activity will increase near the line end and decrease towards the neutral end of the winding, the windows used for antenna placement were selected strategically.

As discussed above, there are a total of 12 circuits in the generator, which means that 12 coils should be at the maximum generator voltage. Every slot contains two half coils; the "top coil" faces the air gap and the "bottom coil" faces the core. As the coil pitch is seven slots, half of each coil is the top coil in one slot and the other half is the bottom coil seven slots away. The antennas used in these experiments were facing the rear of stator winding (bottom coils). As per the winding diagram provided by the manufacturer, 12 slots were found to contain bottom coils connected to the line end. The stator frame windows were examined to see which ones had a direct line of sight to the identified slots (providing the best opportunity for the antennas to detect PD).

Line end coils were visible through windows behind slot 329 (whose bottom coil is part of circuit T5a on A-phase) and slot 118 (whose bottom coil is part of circuit T4a on B-phase). There was no stator frame window providing a direct line of sight to a C-phase line end coil, so the antenna location was chosen behind slot 350 which is ten slots away from the line end of circuit T1a (located in slot 340). The top coil in slot 350 is the fifth coil from the line end. As seen in the window used for A-phase measurements (Fig. 6.6), slots were previously labeled at the rear of the winding. These markings were used to visually identify the slots for this work.

Fig. 6.6: View inside window behind slot 329 for measurement of A-phase PD.

6.3 Results

PD measurements were performed on all six coupling capacitors with the commercial instrument. A summary of the Qm values measured on the three circuits associated with the antenna measurements is found in Table 6.1. PRPD patterns acquired from those circuits are shown in Figs. 6.7, 6.8, and 6.9. The data suggests that larger PD magnitudes are expected from phases B and C. The ambient temperature at the time of these measurements was 35.3°C and the relative humidity was 39.2%. The winding temperature fluctuated between 70°C and 74°C and there was 18 MW of load on the generator.

In this generator, line end coils from different phases are in close proximity to each other. For example, slot 329 (which contains the line end coil of circuit T5a) is close to slot 324 (which contains the line end coil of circuit T1b). If the PD on each circuit is the same, one might expect to detect PD from all phases at once, making it difficult to identify the PD

Table 6.1: Qm values as determined by the commercial instrument.

Phase (Winding Circuit)	Qm+ [mV]	Qm- [mV]
A (T5a//T5b)	27	41
B (T4a//T4b)	250	318
C (T1a//T1b)	224	188

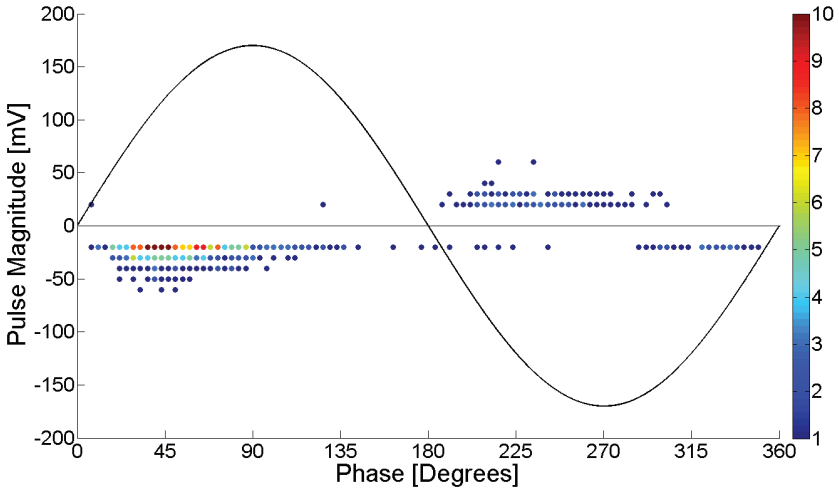

Fig. 6.7: PRPD pattern acquired with the commercial instrument on parallel circuits T5a and T5b (A-phase).

source.

Measurements were performed at the three identified locations using the 900 MHz, 1500 MHz, and 2450 MHz antennas both with and without the conditioning circuit. When the conditioning circuit was not used, PD was not detectable above the noise floor in most cases. Figure 6.10 shows the PRPD pattern obtained with the 2450 MHz antenna placed in front of the designated C-phase coil. Static excitation pulses are present in PRPD patterns acquired with all antennas when the conditioning circuit was not used. Fig. 6.11 shows the waveform and frequency spectrum of one of the pulses from the acquisition depicted in Fig. 6.10. The

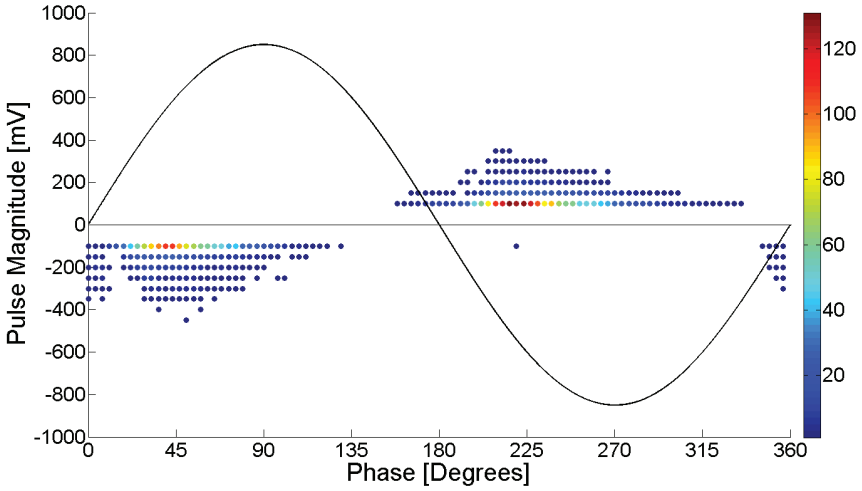

Fig. 6.8: PRPD pattern acquired with the commercial instrument on parallel circuits T4a and T4b (B-phase).

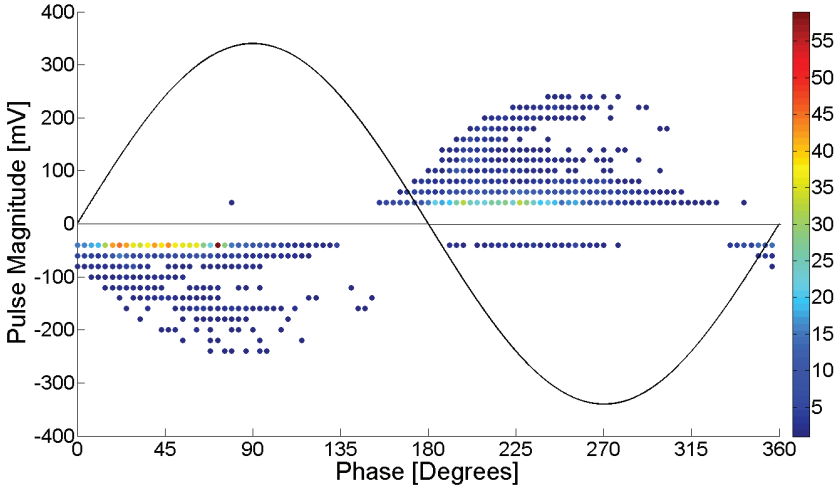

Fig. 6.9: PRPD pattern acquired with the commercial instrument on parallel circuits T1a and T1b (C-phase).

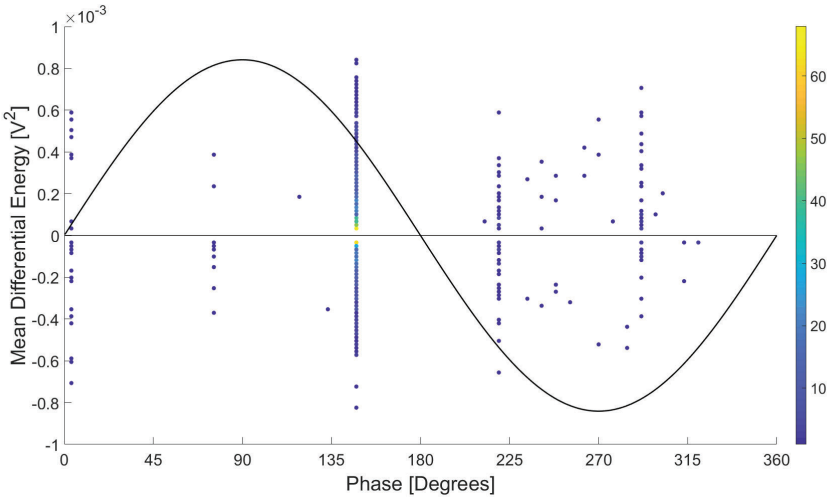

Fig. 6.10: PRPD pattern acquired with the 2450 MHz antenna facing the designated C-phase coil from circuit T1a with no conditioning circuit.

low frequency content suggests that it is not a PD pulse.

Test results improved when measurements were performed with the conditioning circuit. Figure 6.12 shows the PRPD pattern acquired with the 900 MHz antenna measuring PD from the B-phase line end coil. While static exciter pulses are still present, pulse clusters in the first and third quadrants can be identified which indicates PD activity. Figure 6.13 shows the PRPD pattern acquired from the same measurement location except with the 2450 MHz antenna. Similar to the measurement with the 900 MHz antenna, activity in the first and third quadrants appears to be present but the magnitude is lower and the phase-shifted PD activity indicates that PD may have been detected from other phases.

When the 1500 MHz antenna was placed in front of the designated A-phase line end coil, strong PD activity was measured in the third quadrant as shown in Fig. 6.14. This was not expected since there was a negative predominance measured by the commercial instrument (see Fig. 6.7). However, since the commercial instrument detects PD on two parallel circuits

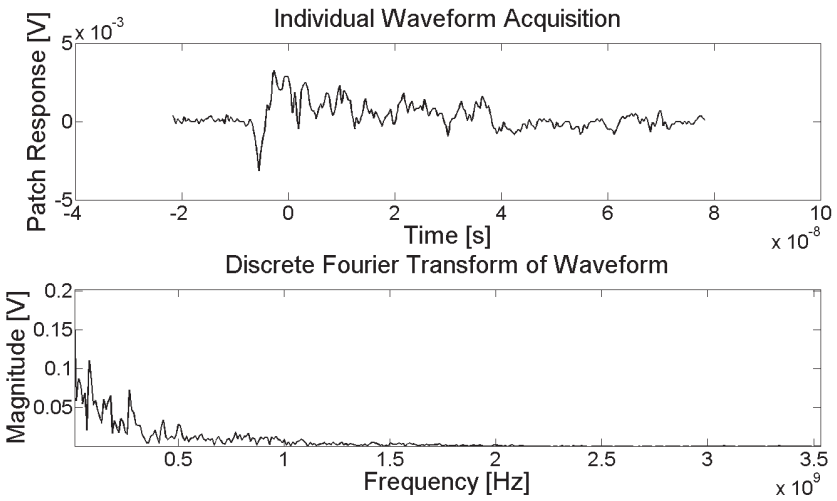

Fig. 6.11: Waveform and spectrum of a PD pulse acquired on the designated C-phase coil with the 2450 MHz antenna.

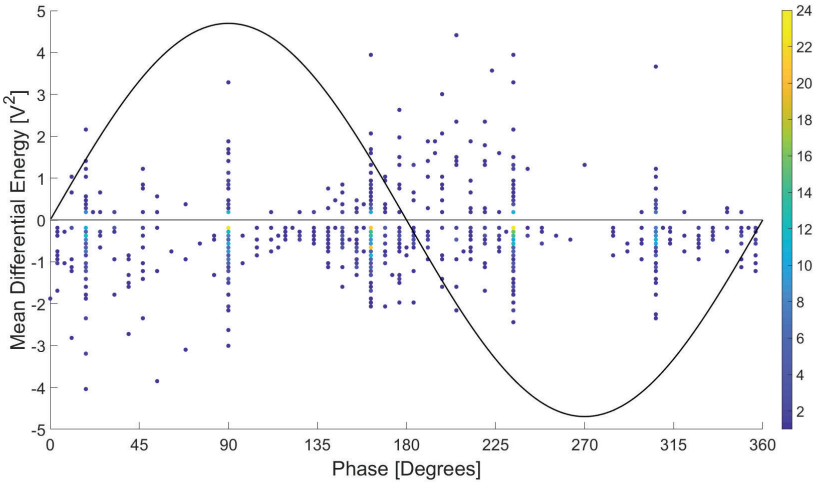

Fig. 6.12: PRPD pattern acquired with the 900 MHz antenna facing a line-end coil on B-phase circuit T4a with a conditioning circuit.

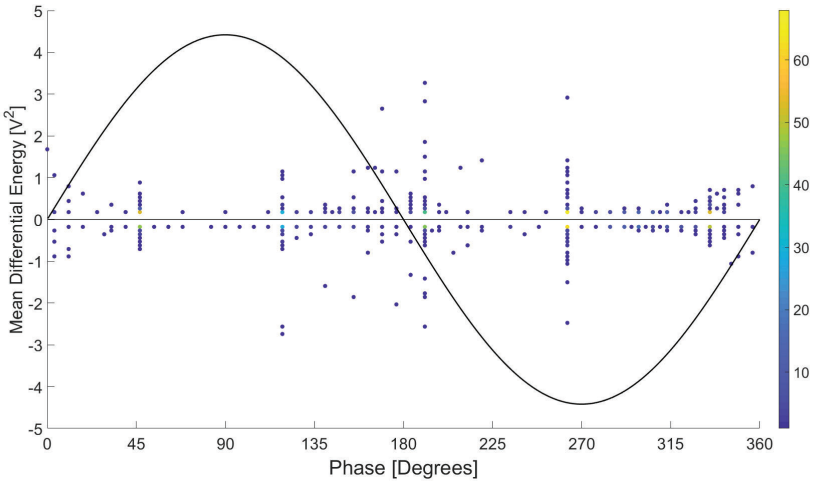

Fig. 6.13: PRPD pattern acquired with the 2450 MHz antenna facing a coil on B-phase circuit T4a with a conditioning circuit.

simultaneously, it is not possible to determine whether T5a has negative predominance. Figure 6.14 also contains PD activity in the third quadrant which may be from other phases. Figure 6.15 provides evidence that the 1500 MHz antenna detected activity radiating at the antenna's resonant frequency.

6.4 Conclusions from Field Experiments

The results presented in this chapter confirm that it is possible to detect PD with UHF antennas on generators operating in a powerhouse. Measurements were performed with no outage (required for installation of sensors used with conventional measurement systems). Time to set up and perform tests with the antennas was comparable to the time required to perform measurements with the commercial instrument.

Similar to laboratory measurements discussed in Chapter 5, there were issues with test

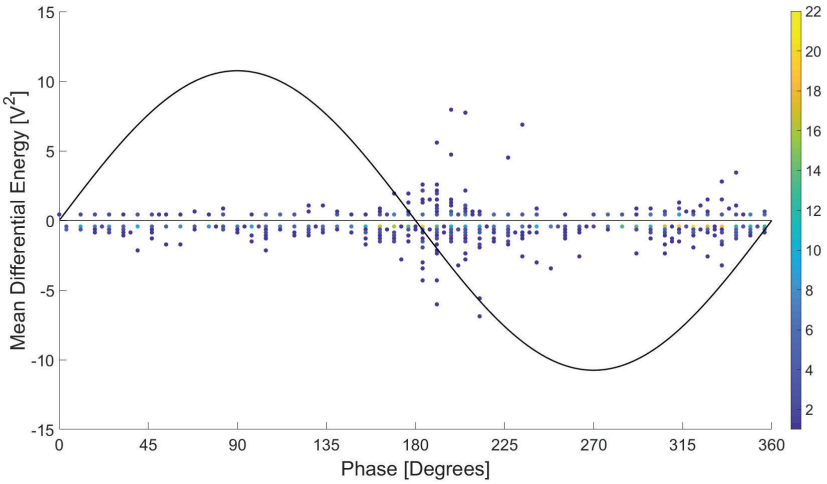

Fig. 6.14: PRPD pattern acquired with the 1500 MHz antenna facing a line-end coil on A-phase circuit T5a with a conditioning circuit.

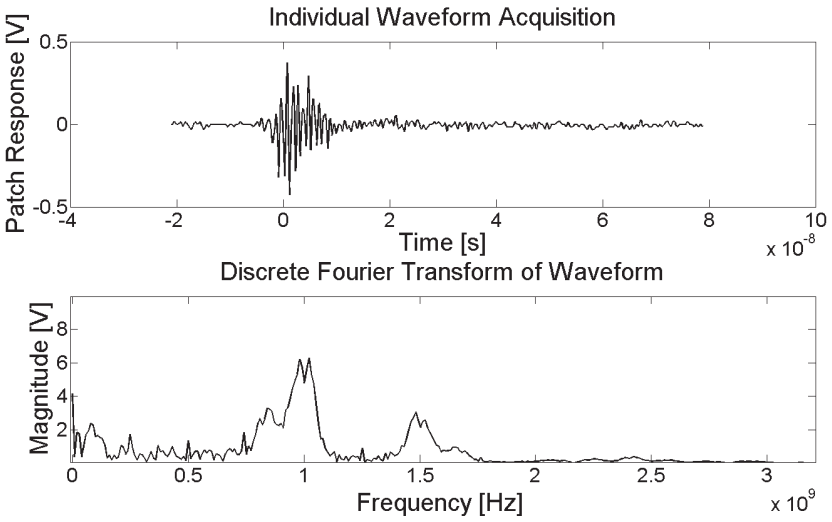

Fig. 6.15: Waveform and spectrum of the acquisition with the 1500 MHz antenna facing the line-end coil on A-phase circuit T5a with a conditioning circuit.

quality and reliability due to the manual adjustment of trigger settings. Since the PRPD patterns were generated in post-processing, it was difficult to verify that the selected trigger setting was appropriate for each acquisition. The antennas were sensitive to static excitation pulses which have lower frequency content than PD pulses. Therefore, the incoming pulse shape was used to verify the trigger settings. This method of data acquisition is not reliable and should be improved for future work.

An outstanding problem that remains to be solved is that microstrip patch antennas placed near a stator endwinding will inevitably detect PD from other phases. In this work, PD was detected from multiple phases. Additionally, the windows in the stator frame that provided a line of sight to the stator winding are not available on all generators.

Chapter 7
Conclusions and Future Work

7.1 Concluding Remarks

This thesis demonstrated that it is possible to detect PD in the UHF range that is radiated from a stator winding operating in a generating station. There was agreement between PRPD patterns obtained with the antennas and those obtained with a commercial instrument. It was found that in the generating station, a signal conditioning circuit was required to detect PD due to the prevalence of switching disturbances from the static excitation system.

Measurements performed with the 2450 MHz antenna were much less sensitive to PD than the other two antennas, therefore it should not be used for future work. However, laboratory PD was measured in the far field with all three antennas, except at antenna position P3.

Laboratory measurements at antenna positions P1 and P2 yielded similar results. Most measurements in the P3 position had poor results. This is of no consequence because it would not be practical to install a patch antenna in that position anyway since it would have to be placed on the stator or rotor surface in the air gap.

While there was attenuation of the measured signal with increasing antenna distance (as expected), the information in the PRPD patterns remained the same regardless of distance. The maximum antenna distance at which PD was still measurable depended on the specimen and the magnitude of the radiated PD.

7.2 Future Work

7.2.1 Improvements to Data Acquisition and Processing

While the methods for acquiring and processing PD pulses were suitable for this thesis, there were issues encountered (discussed in Chapters 5 and 6) due to flaws in the measurement setup.

The biggest flaw was that measurement quality was highly dependent on oscilloscope trigger settings. In addition, there was no way to be certain that the trigger setting used for any given experiment was appropriate until after post-processing. This resulted in many unreliable acquisitions and a considerable amount of time repeating tests. To solve this problem, the digital oscilloscope can be connected to a laptop for real-time processing so that a PRPD pattern can be populated as the oscilloscope is being adjusted. This feature is available in the commercial instruments PDBase and PDCheck developed by TechIMP (which does not involve the use of UHF antennas).

Another flaw has to do with the method of generating PRPD plots. By using the Mean Differential Energy, an assumption was made that all noise was symmetrical and the resulting signal energy was representative of the PD signal. This was never proven to be correct. If the noise/ringing in any pulse is asymmetrical, the accuracy of the resulting pulse polarity and magnitude would be skewed. To rectify this issue, peak-hold circuitry can be implemented

similar to that found in the IRIS TGA-BP instrument. This would ensure that the first peak of the pulse is recorded to calculate the PD magnitude. In this thesis, PRPD patterns obtained with the UHF antennas had pulse polarity that was mostly in agreement with commercial data.

7.2.2 Optimization of the Antenna

The rectangular patch antenna is not directional. This can be a problem for online stator winding measurements since PD is being measured from individual bars or coils. If PD from all three phases is detectable by the antenna, it could be challenging to separate PD activity on each phase. The results in Chapter 6 indicate that multi-phase PD may have been detected on Great Falls Unit 1. Therefore, future experiments should be performed with a highly directional antenna. Additional antennas and a spatial difference technique, such as the one used in [34], may be required.

7.2.3 Further Experimentation and Other Applications

Since measurements in this thesis were promising, more experiments in the laboratory and in the field should be performed to build a larger body of data to further evaluate this technique. The conventional methods of online rotating machine PD measurement are highly established and it would be challenging to convince utilities to adopt a new technique unless there is a distinct economic advantage. In addition, locations for antenna placement on machines that do not have an easily accessible line of sight to their stator windings (such as hydrogen-cooled machines, for example) should be determined.

This thesis focused on rotating machine winding PD, but the measurement technique can be applied to other high voltage assets (i.e. transformers, breakers, etc.). A major advantage

of this technique is that it does not require an outage which can be prohibitively expensive for a utility. For other assets such as instrument transformers, PD acceptance limits have been established in picocoulombs using conventional narrowband measurement methods. To use UHF antennas for PD measurements on these assets, specific methods would have to be established to calibrate measured PD to apparent charge in pC (if this is possible).

Another possible application for the antennas is inspired by the research conducted by IREQ (L'Institut de recherche d'Hydro-Québec) on Roebel bars in the laboratory [43, 44]. In this research, the TVA probe (see Section 2.3.2) was used to localize PD in a bar by measuring the resulting peak current at various locations along the bar. Perhaps since the UHF antennas operate at higher frequencies, they can perform the same function with higher accuracy.

References

[1] G. Stone, "IRIS Power Partial Discharge Seminar - Electrical Rotating Machine Stator Windings," *PD Theory, Detection and Interpretation, Version 5.2*, 2014.

[2] G. Stone, E. Boulter, I. Culbert, and H. Dhirani, *Electrical Insulation for rotating machines: design, evaluation, aging, testing, and repair.* Piscataway, NJ:IEEE; Hoboken, NJ: Wiley-Interscience: Wiley/IEEE, 2004.

[3] B. Guru and H. Hiziroglu, *Electric machinery and transformers.* New York, NY: Oxford University Press, 2001.

[4] "IEEE Guide for the Measurement of Partial Discharges in AC Electric Machinery," *IEEE Standard 1434-2014*, 2014.

[5] R. Bartnikas, "Partial Discharges - Their Mechanism, Detection and Measurement," *IEEE Transactions on Dielectrics and Electrical Insulation*, vol. 9, no. 5, pp. 763–808, October 2002.

[6] "High Voltage Test Techniques - Partial Discharge Measurements," *IEC International Standard 60270*, 2015.

[7] "On-line partial discharge measurements on the stator winding insulation of rotating electrical machines," *IEC International Standard 60034-27-2*, 2012.

[8] "IEEE Recommended Practice for Measurement of Power Factor Tip-Up of Electric Machinery Stator Coil Insulation," *IEEE Standard 286-2000*, 2000.

[9] S. Hoek, A. Kraetge, M. Kruger, S. Korber, O. Kessler, and B. Battle, "Acoustic partial discharge localization in combination with electrical measurements applied on power transformer," in *Proceedings of Advanced Research Workshop on Transformers*, 2013.

[10] L. Fornasari, G. Montanari, and A. Cavallini, "Alarm Management in Permanent PD Monitoring for Generators," in *Proceedings of IEEE International Symposium on Electrical Insulation*, 2012.

[11] *MONGEMO - Permanent on-line partial discharge monitoring system for power generators and electrical motors.* Omicron, 2016.

[12] M. Partyka, G. Bridges, B. McDermid, T. Black, and B. Kordi, "UHF Measurement of Partial Discharge on Stator Bars Using Patch Antennas," in *Proceedings of IEEE Electrical Insulation Conference*, June 2019, pp. 453–456.

[13] A. Pemen, P. van der Laan, and W. de Leeuw, "Propagation of partial discharge signals in stator windings of turbine generators," *IEEE Transactions on Energy Conversion*, vol. 21, no. 1, pp. 155–161, March 2006.

[14] G. Stone, H. Sedding, C. Chan, and C. Wendel, "Comparison of Low Frequency and High Frequency PD Measurements on Rotating Machine Stator Windings," in *Proceedings of IEEE Electrical Insulation Conference*, June 2018, pp. 349–352.

[15] *PDA-IV: Periodic Online Partial Discharge Monitoring Instrument for Hydro Generators.* IRIS Power, 2016.

[16] *A comprehensive approach to Generator condition assessment enabling predictive maintenance.* General Electric, 2016.

[17] *RMM: Rotating Machine Monitor.* Dynamic Ratings, 2013.

[18] G. Stone and H. Sedding, "Comparison of UHF Antenna and VHF Capacitor PD Detection Measrurements from Turbine Generator Stator Windings," in *Proceedings of IEEE International Conference on Solid Dielectrics*, July 2013, pp. 63–66.

[19] *Stator Slot Couplers.* IRIS Power, 2015.

[20] H. Sedding, G. Stone, and G. Klempner, "A New Sensor for Detecting Partial Discharges in Operating Turbine Generators," *IEEE Transactions on Energy Conversion*, vol. 6, no. 4, pp. 700–706, December 1991.

[21] H. Sedding, G. Stone, S. Campbell, and G. Klempner, "Evaluation of Coupling Devices for In-Service Partial Discharge Detection of Thermal Alternators," in *CEA 738 G 631*, November 1992.

[22] D. M. Pozar, *Microwave Engineering, 4th Edition.* John Wiley and Sons, Inc., 2012.

[23] T. Dakin, C. Works, and J. Johnson, "An Electromagnetic Probe for Detecting and Locating Discharge in Large Machine Stators," *IEEE Transactions on Power Apparatus and Systems*, vol. 88, no. 3, pp. 251–257, March 1969.

[24] C. Balanis, *Antenna Theory*, 3rd ed. John Wiley and Sons, Inc., 2005.

[25] A. Cavallini, G. Montanari, R. Candela, and L. Testa, "Partial discharges detection in medium voltage systems using directional antenna sensors," in *IEEE Conference on Electrical Insulation Dielectric Phenomena*, 2008.

[26] U. Khayam and F. Alfaruq, "Design of Hilbert antenna as partial discharge sensor," in *International Conference of Industrial, Mechanical, Electrical, and Chemical Engineering (ICIMECE)*, 2016.

[27] A. Suryandi and U. Khayam, "New designed bowtie antenna with middle sliced modification as UHF sensor for partial discharge measurement," in *Proceedings of International Conference on Smart Green Technology in Electrical and Information Systems (ICSGTEIS)*, 2014.

[28] U. Khayam and F. Fatoni, "Measurement of partial discharge induced electromagnetic wave using loop antenna," in *Proceedings of International Conference on Electrical Engineering, Computer Science and Informatics (EECSI)*, 2017.

[29] F. Nugraha, N. Harid, B. Barkat, N. A. Sayari, S. Jayaram, and H. Griffiths, "Analysis of partial discharge in air using emitted electromagnetic waves and the HFCT method," in *Proceedings of IEEE Electrical Insulation Conference*, 2016.

[30] A. Contin and D. Geremia, "PD detection in rotating machines using a portable instrument based on an antenna probe," in *Proceedings of IEEE Electrical Insulation Conference (EIC)*, 2017.

[31] Y. Tao, J. Wang, and Z. Xu, "Design, simulation and test of a double differential d-dot overvoltage sensor," *International Journal of Applied Electromagnetics and Mechanics*, vol. 58, no. 2, pp. 1–19, January 2015.

[32] X. Zeng, H. Li, Y. Lu, and Y. Chen, "Online monitoring of partial discharge in high voltage switchgear using a differential electric field sensor," in *Proceedings of IEEE Conference on Electrical Insulation and Dielectric Phenomenon (CEIDP)*, 2017.

[33] G. Hussain, M. Shafiq, M. Lehtonen, and M. Hashmi, "Online Condition Monitoring of MV Switchgear Using D-dot Sensor to Predict Arc-Faults," *IEEE Sensors*, vol. 15, no. 12, pp. 7262–7272, December 2015.

[34] M. Kawada, Z. Kawasaki, K. Matsu-Ura, S. Kuroki, T. Osawa, and H. Tanaka, "On-Line Partial Discharge detection of Turbine Generator Using Gigahertz-Band Spatial Phase Difference Method," *Electrical Engineering in Japan*, vol. 131, no. 4, pp. 38–43, November 2000.

[35] M. Kawada and Z. Kawasaki, "Insulation Diagnostic Technique to Assess the Condition of Generator Winding by Measuring Microwave Associated with Dielectric Breakdown," *IEEE Transactions on Dielectrics and Energy Conversion*, vol. 15, no. 1, pp. 19–23, March 2000.

[36] M. Kawada, Z. Kawasaki, K. Matsuura, S. Kuroki, T. Osawa, and H. Tanaka, "Detection of partial discharge in operating turbine generator using GHz-band spatial phase difference method," in *Proceedings of International Symposium on Electrical Insulating Materials*, 1998.

[37] H. Muto, Y. Kaneda, H. Aoki, and O. Hamamoto, "On-line PD monitoring system for rotating machines using narrow band detection of EM wave in GHz range," in *Proceedings of International Conference on Condition Monitoring and Diagnosis*, 2008.

[38] Y. Shibuya, S. Matsumoto, M. Tanaka, H. Muto, and Y. Kaneda, "Electromagnetic waves from partial discharges and their detection using patch antenna," *IEEE Transactions on Dielectrics and Electrical Insulation*, vol. 17, no. 3, pp. 862–870, June 2010.

[39] W. Ediriweera, K. Priyanayana, R. Rajakaruna, R. Ranasinghe, J. Lucas, and R. Samarasinghe, "Microstrip patch antenna for partial discharge detection as a condition monitoring tool of power system assets," in *Proceedings of Moratuwa Engineering Research Conference (MERCon)*, 2017.

[40] D. Mishra, B. Sarkar, C. Koley, and N. Roy, "Characterisation of Microstrip patch antenna based UHF sensor for detection of partial discharge," in *Proceedings of IEEE India Conference (INDICON)*, 2015.

[41] B. Sarkar, C. Koley, N. Roy, and P. Kumbhakar, "Low cost rf sensor for partial discharge detection of high voltage apparatus," in *Proceedings of IEEE International Conference on Condition Assessment Techniques in Electrical Systems (CATCON)*, 2013.

[42] M. Ashtiani and S. Shahrtash, "Partial Discharge Pulse Localization in Excessive Noisy Data Window," *IEEE Transactions on Dielectrics and Electrical Insulation*, vol. 22, no. 1, pp. 428–435, February 2015.

[43] C. Hudon, M. Levesque, S. Bernier, H. Provencher, E. Cloutier-Rioux, and Y. D. Seol, "Scanning Individual Stator Bars and Coils with an Antenna to Detect Localized Partial Discharges," in *Proceedings of IEEE Electrical Insulation Conference*, June 2019, pp. 457–460.

[44] E. Cloutier-Rioux, H. Provencher, A. Turgeon, and C. Hudon, "Calculation of the Electric Field Inside Cavities Found Through Stator Bar Dissection," in *Proceedings of IEEE Electrical Insulation Conference*, June 2019, pp. 129–132.